UNIVERSITA' DEGLI STUDI DI TORINO

Dipartimento di Scienze Mediche

DOTTORATO DI RICERCA IN FISIOPATOLOGIA MEDICA

Ciclo XXXII

TESI DI DOTTORATO

Mesenchymal Stem Cell derived extracellular vesicles modulate fibrosis and autophagy in a model of diabetic nephropathy

Tutor
Prof. Maria Felice Brizzi

PhD Candidate
Dott.ssa Marta Tapparo

INDEX

Abstract **pag.1**
Introduction ..... **pag. 2**
Diabetic nephropathy pag.2
Hemodynamic factors pag.5
Hypoxia and oxidative stress pag.7
Inflammation pag.7
Fibrosis pag.8
Autophagy pag.11
Autophagy and kidney fibrosis pag.12
Stem cell derived extracellular vesicles and regenerative medicine pag.13
AIM OF THE STUDY **pag.16**
MATERIALS AND METHODS **pag.17**
Cell Culture pag.17
Isolation and characterization of EVs pag.17
Proteomic analysis by antibody-based protein array pag.18
miRNome analysis pag.18
Bioinformatic analysis pag.18
Mouse model of diabetic nephropathy pag.18
Biochemical and histological analyses pag.19
Immunofluorescence pag.20
TUNEL pag.20
Transcriptomic analysis of kidney tissue pag.20
PCR arrays ..... pag 20
Real time PCR pag.21
Western blot pag.22
Statistical analysis pag.22
RESULTS **pag.23**
MSC EV morphology and surface markers characterization pag.23
MSC EV protein cargo analysis pag.23
MSC EV miRNA cargo analysis pag.27
MSC EVs ameliorate renal function and decrease renal fibrosis (curative model) pag.32
MSC EVs decrease and partially revers renal fibrosis in ND mouse model pag.34
MSC EV treatment ameliorate fibrosis soon after diabetes onset pag.36
MSC EVs slightly modulate autophagy in DN renal tissue pag.38

MSC EV cargo could modulate the autophagy cascade.....pag.41
DISCUSSION..... pag.44
CONCLUSION..... pag.48
REFERENCE pag.49

ABSTRACT

Introduction: Diabetic nephropathy (DN) is a complex disease and one of the major cause of end-stage renal disease (ESRD). DN is characterized by glomerular hypertrophy and hyperfiltration that cause microalbuminuria. In diabetic setting, persistent hyperglycaemia and the formation of advanced glycation end-products (AGE) activate cellular stress pathways favouring the release of pro-inflammatory and pro-fibrotic cytokines. All these events lead to glomerular and tubule-interstitial inflammation, mesangial cell and myofibroblast expansion and fibrosis. In the recent years, different therapeutic strategies have been investigated to ameliorate kidney injury and fibrosis. Mesenchymal stem cells (MSC) and in particular their derived extracellular vesicles (MSC EVs) have been considered attractive therapeutic options due to their efficacy in different therapeutical application and low immuogenicity. It has been shown that MSC EVs contain several RNA species, including mRNAs, microRNAs (miRNAs) and long non-coding RNAs that transferred to target cells may induce epigenetic changes and functional effects. Proteins and lipids carried by EVs, are also relevant for multi-organ development, cell survival and differentiation as well as for tissue repair.

Aim: In the present study, the regenerative potential of MSC derived EVs was investigated in a mouse model of DN. Their potential role in preventing progression of kidney fibrosis and the modulation of the signalling associated with autophagy were evaluated.

Methods: Diabetes was induced in NSG mice by streptozotocin injection. MSC-derived EVs were administered weekly to diabetic mice for four weeks soon after diabetes onset or after one month after DN development. Kidney fibrosis and autophagy were evaluated in kidney and the expression of fibrosis and autophagy related genes were analysed. MSC EV cargo, as miRNA and protein content, was also analysed to identify molecules potentially involved in their protective effects.

Results: MSC EV treatment significantly ameliorated functional parameters, such as albumin/creatinine ratio, plasma creatinine and blood urea nitrogen. Moreover, MSC EV-treated animals showed a significant reduction of kidney fibrosis confirmed by trichrome staining and by the expression of fibrotic genes whose level was partially restored. We also investigated the modulation of genes involved in autophagy by PCR array on kidney of DN mice treated one week after diabetes onset and sacrificed at week 4. MSC EVs seems to regulate the expression of key genes involved in the formation of the autophagosome and in the regulation of mTOR/PI3K pathway. All these data suggest that MSC EVs are effective in preventing DN progression. EV miRNA content was characterized and target prediction analyses demonstrated that MSC EV treatment was associated with the modulation of mTOR/PI3K, VEGF, TGFβ and AMPK pathways. Moreover, p53-apoptosis, cell cycle and ECM-receptor interaction pathways were found associated with predicted target genes for MSC EV specific miRNAs. Screening of MSC EV protein cargo identified the presence of molecules mainly related to signal transduction, cell communication, immune response and cell growth and maintenance. Among them, we identified some transcription factors such as CREBBP and PPARG that modulate TGFβ and the Wnt signalling.

Conclusion: These results indicate that in diabetic setting, MSC EV administration ameliorate kidney injury by different mechanisms.

INTRODUCTION

Diabetic nephropathy

Diabetic nephropathy (DN) is a clinical syndrome that occur as long term diabetes complication. Diabetes (DM) occurs due to lack of insulin production or insulin sensitivity. It is mainly classified into many types, however, the most common types are type 1 and type 2 DM. Type 1 DM (T1DM) is an autoimmune disorder in which T lymphocyte react against pancreatic β-cell causing a reduction of insulin secretion [1]. On the other hand, type 2 DM (T2DM) is characterised by insulin resistance and reduction of insulin production. Both types leads to an increase of blood glucose concentration and long term exposure cause metabolic disregulation and vascular alterations [1].

Approximately 20-40% patients with diabetes mellitus develop nephropathy with a significant proportion requiring regular dialysis or renal replacement therapy (RRT) [2, 3], however, these approaches have limitations, including high costs and organ availability [4].

DN is clinically defined by persistent albuminuria with a progressive decline in renal function and characterized by a typical pattern of glomerular disease.

Patients that develop nephropathy show microalbuminuria (persistent albuminuria at level 30–299 mg/24 hours). Macroalbuminuria (persistent albuminuria at level >300 mg/24 hours) occur after many years in type 1 diabetes, but may be present at the time of diagnosis in type 2 diabetes and these patients usually develop end-stage-renal-disease (ESRD) [5]. However, in the last years the classification of kidney disease severity is based on albumin-to-creatinine ratio (ACR). A moderate disease correspond to micro-albuminuria (30 to 300 mg/g or 3 to 30 mg/mmol) that becomes severe in patients with ACR>300mg/g or 30 mg/mmol, corresponding to macroalbuminuria [6].

In the early stage, typical DN features mainly involve the glomerulus and include podocyte damage/loss and mesangial and interstitial hypertrophy. Subsequently increased synthesis of extracellular matrix (ECM) proteins, such as fibronectin and collagen, leads to glomerular basement membrane thickening, tubule-interstitial fibrosis and tubular atrophy [3]. Arteriolar hyalinosis and arteriosclerosis are also commonly detected (Figure 1).

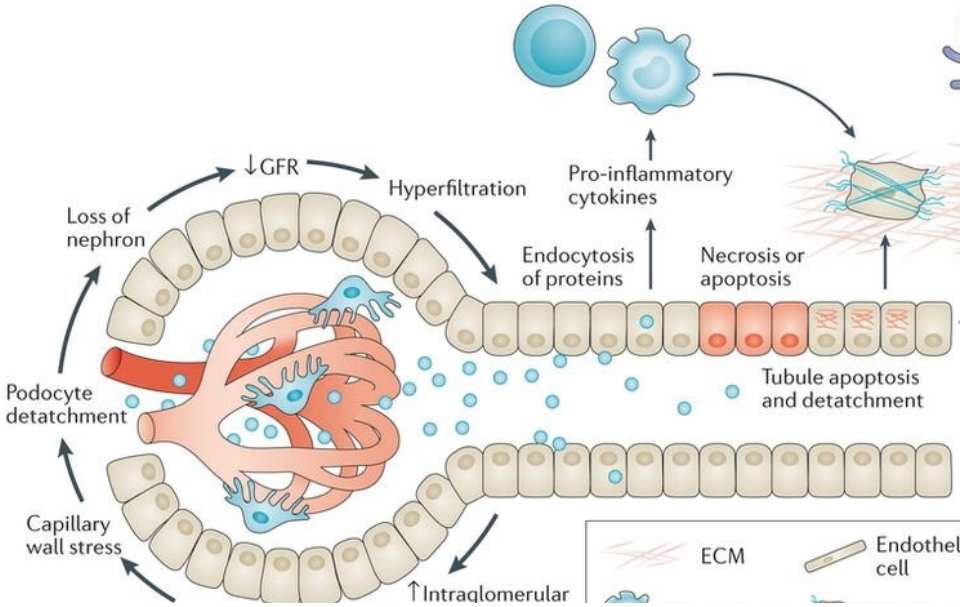

Figure 1. Diabetic nephropathy features. Glomerular hyperfiltration is associated with glomerular hypertrophy, which results in podocyte detachment and loss. Loss of podocytes causes albuminuria and glomerulosclerosis, and leads to glomerular hypertrophy and self-sustaining nephron loss. Hyperglycaemia, increased the levels of fatty acids and proteinuria cause epithelial damage and cell death, detachment, dedifferentiation of epithelial cells, and increased expression of pro-inflammatory cytokines. Increased cytokine expression leads to macrophage and T cell recruitment. Epithelial damage also induces myofibroblast transformation and production of extracellular matrix (ECM). GFR, glomerular filtration rate [from Edeling 2016, Nature reviews].

Podocytes are highly differentiated epithelial cells that reside in the glomerulus and, along with glomerular endothelium and glomerular basement membrane (GBM), are relevant for the formation of the glomerular filtration barrier (GFB) [8].

Hyperglycaemia can induce podocyte apoptosis. Since their regenerative capacity is low, podocytopenia might be irreversible, thus leading to permanent damage [9]. The induction of apoptosis is mediated trough different mechanisms such as excessive ROS production, renin-angiotensin-aldosterone-system (RAAS) activation, mammalian target of rapamycin (mTOR) pathway, transforming growth factor-β (TGF-β)/SMAD, or advanced glycation end-products (AGE) activated pathways [3]. Podocytopenia induce loss of GBM integrity which on turn results in increased albuminuria tubular cell injury and the development of fibrosis. Besides podocyte loss, foot process effacement (FPE) is a common histological feature in DN patients. FPE is associated with high level of albuminuria and loss of nephrin expression on slit diaphragms [10]. Urinary nephrin excretion was observed in the 30% of normoalbuminuric, 17% of microalbuminuric, and 28% of macroalbuminuric T1DM patients whereas none of the healthy subjects had nephrinuria [11]. Nephrin expression was shown to be controlled by histone deacetylase 4 (HDAC4) [12] whose expression is induced by high glucose. HDAC4 causes deacetylation of nephrin, that is degraded through ubiquitin and 26S

proteaosome pathwas [12]. In contrast, expression of CD2AP, another podocyte-specific protein, is not reduced in podocytes from diabetic patients, suggesting that the observed reduction in nephrin is not due to general loss or major injury of podocytes [11]. Lin et al. showed that Notch-1 is involved in podocytes dysfunction during diabetic proteinuria development. Experimental model in human podocytes, human embryonic kidney (HEK)-293 cells and within the glomeruli of diabetic rats showed that when high glucose activates Notch-1 signalling, VEGF expression increased whereas nephrin expression is reduced cuasing podocyte apoptosis [12].

Historically increased albuminuria and glomerular changes are described as early sign in DN while tubule-interstitial events occur later. However, different studies have demonstrated that tubular damage occur early in DN and may be very critical for renal disease progression [13]. Vaidya *et al*., have described that at baseline tubular injury biomarkers such as kidney injury molecule-1 (KIM-1) and N-ßacetyl-D-glucosaminidase (NAG) are associated with regression of microalbuminuria [14], while KIM-1 is significantly associated with the risk of early renal function decline, independently of albuminuria. All these clinical parameters suggest that tubular damage play a role in the development of DN and may precede and influence glomerular changes [15]. This long lasting tubular injury can lead to inflammation and fibrosis.

As extensively reported, DN progression also depends on hemodynamic and metabolic factors, hypoxia, oxidative stress, and inflammation contributing to activation of different cell signalling.

Changes in the signalling pathways lead to dysregulation of the expression of transcription factors controlling ECM homeostasis and drive glomerular and tubule-interstitial fibrosis [16-18] (Figure 2).

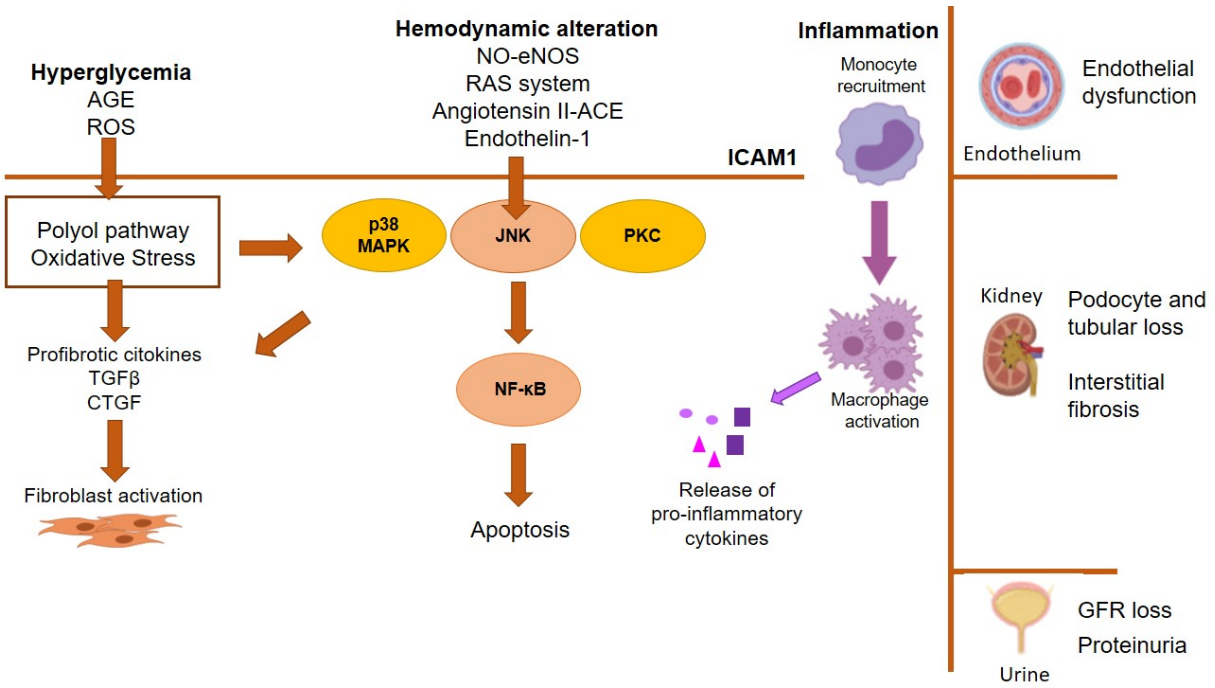

Figure 2. Factors and pathways involved in DN pathogenesis.

Hemodynamic factors

Endothelial dysfunction is crucial for DN development, and involves interstitial peritubular capillary vessels as well as the glomerular afferent and efferent arterioles. [19]. Nitric Oxide (NO) is one of the key factor produced by endothelial nitric oxide synthase (eNOS) and involved in vascular homeostasis maintenance, including vascular tone, leukocyte adhesion to endothelium, proliferation of vascular smooth muscle cells, and platelet aggregation and adhesion to the vessel. Tessari *et al*. demonstrated, in a diabetic setting, that reduction of NO by knocking-down eNOS, caused glomerular endothelial injury and results in overt albuminuria and glomerular mesangiolysis [20]. Insulin resistance can also inhibit insulin receptor signaling leading to reduction of NO synthesis [21]. Genetic polymorphisms causing reduced production of NO are reported to accelerate the progression of DN [22].

Moreover, NO induces vasodilation of the afferent and efferent arterioles, while the imbalance between afferent and efferent arteriolar resistance increases glomerular hydrostatic pressure and hyperfiltration, leading to glomerular damage[23].

Many studies have demonstrated that the iperactivation of RAAS contributed to both systemic and regional glomerular capillary hypertension, which could induce hemodynamic injury to the glomerulus, leading to kidney damage and progression of renal fibrosis [24]. Plasma angiotensinogen is cleaved by renal renin, generating angiotensin I (AngI), which is then converted to angiotensin II (AngII) by endothelial angiotensin-converting enzyme (ACE). AngII is considered the most important RAAS peptide and is associated with vasoconstriction and high blood pressure. AngII binds to the type–1 AngII receptor (AT1) in a variety of

tissues. Then, aldosterone is stimulated via the AT1 receptor in the adrenal gland, facilitating sodium retention by the kidney when aldosterone binds to the mineralocorticoid receptor. The activation of RAAS increases angiotensin II levels, and leads to vasoconstriction of the efferent arteriolar and the production of pro-inflammatory and pro-fibrotic molecules through multiple mechanisms. In diabetic mice and humans high level of angiotensin converting enzyme (ACE) correlates with the increased albuminuria and kidney injury [25]. The use of RAAS antagonists, like ACE inhibitors and angiotensin receptor blocker (ARB) prevented renal fibrosis and slowed the progression to ESRD. Some new non-peptide drugs that modify RAAS activity have been developed, including several novel agonists (such as AT2R agonists and MAS1 agonists) and antagonists (such as AT4R inhibitors) of the RAAS, some of which have entered clinical applications and some of which are still in the stage of clinical trials [24].

Many studies showed that the level of the vasoactive hormone, endothelin-1 (ET-1), was significantly elevated in DN and contributes to worsen the vascular resistance [26]. ETs are 21-amino acid vasoconstrictive peptides produced primarily in the endothelium and have key roles in vascular homeostatsis. ET-1 is the best known and predominant isoform produced in the cardiovascular system and kidney. ET-1 is generally not stored and released, but instead generated in response to a range of stimuli, and is a potent mitogen in vascular smooth muscle cells and mesangial cells. Gene transcription of ET-1 is enhanced during conditions of renal stress, such as hypoxia, inflammation, hyperglycemia, and acidosis, suggesting ET-1 involvment in CKD pathophysiology [27]. ET antagonism with a selective endothelin A receptor (ETA) antagonist attenuates collagen deposition and renal vascular and glomerular fibrosis in several forms of experimental hypertension. However, observations from clinical studies indicate that these antagonists also elicit volume-related side effects [27].

Persistent hyperglycaemia, besides contributing to endothelial cell dysfunction, can induce cell apoptosis through the activation of NF-κB and c-Jun NH2-terminal (JNK) pathways [28]. Vascular rarefaction can lead to chronic hypoxia which by itself induces endothelial cell apoptosis and sustains the injury. Moreover, the interaction between endothelial cells and pericytes is essential for vessel stabilization and pericytes shift into myofibroblasts drives pericyte/endothelial cell detachment and the induction of fibrotic events leading to CKD [29]. A number of studies have reported the increase of vascular endothelial growth factor (VEGF)-A in DN mice [30]. VEGF is constitutively expressed by podocytes and acts on glomerular endothelial cells by binding to its receptors VEGFR1 and VEGFR2. VEGF-A level is tightly regulated to maintain the integrity of the glomerular structure. It has been demonstrated that VEGF-A expression in podocytes of healthy mice recapitulates distinctive DN features such

as proteinuria, glomerulomegaly, GBM thickening, mesangial expansion and podocyte effacement [31].

Hypoxia and oxidative stress

Cortical and medullary hypoxia have been reported in humans with DN and it is known to play a role in the development of CKD [32]. The increased expression of the hypoxia induced transcription factor, hypoxia-inducible factor (HIF)-1α, has been reported to contribute to fibrogenesis [33]. Moreover, during hypoxia, diabetic proximal tubular cells are more susceptible to mitochondrial dysfunction caused by the impairment of mitochondrial dynamics of fission and fusion that led to a delayed recovery of kidney injury [34]. Chronic exposure to high glucose (as occurs in diabetes) resulted in mitochondria disruption, which has been associated with reduced respiration and decreased mitochondrial superoxide production (consider as an indicator of mitochondrial activity) and ATP generation [34].

High glucose concentration leads to the formation of AGE which alter the structures and functions of different molecular species such as proteins, lipids, and nucleic acids by activating both the oxidative stress and the pro-inflammatory pathways [35]. Oxidative stress and generation of reactive oxygen species (ROS) activate the protein kinase C (PKC), the mitogen activated kinase (MAPK), and the NF-κB pathways associated with cellular stress [36]. Furthermore, excess of free glucose activates the polyol pathways translating in the increase production of sorbitol and fructose by sorbitol dehydrogenase. This on turn contributes to boost oxidative stress by increasing the NADH/NAD+ ratio [37].

Inflammation

Inflammation is an additional hall mark of DN and plays an important role in the progression toward ESRD. Macrophages and T-lymphocytes are the most relevant cell population detected in glomeruli at the early stage of diabetes, while interstitial infiltrates can be later detected.

Hyperglycaemia and AGE induce the expression of adhesion molecules and chemokines in proximal tubular cells [38,39] generating an inflammatory milieu which attracts neutrophils, monocytes, and macrophages [40].

Upregulation of the key leukocyte adhesion molecule, the Intercellular Adhesion Molecule 1 (ICAM-1), on endothelial cells facilitates the infiltration of circulating mononuclear cells into the kidney. Additional factors such Colony Stimulating Factor 1 (CSF-1), which promotes monocyte/macrophage differentiation, proliferation, and activation, and Macrophage migration inhibitory factor (MIF), which retains macrophages at sites of inflammation, have

been also described [40]. Accumulation of interstitial macrophages strongly correlates with proteinuria, interstitial fibrosis, and the decline of glomerular filtration rate (GFR) [40].

In hyperglycaemic setting, migration of T lymphocyte to the kidney was also described [41]. ICAM-1 and the Monocyte Chemoattractant Protein-1 (MCP-1/CCL2) mediate their attraction to the kidney and activate both interferon-γ (IFN-γ) and tumor necrosis factor (TNF)-α secretion by lymphocytes, thus activating endothelial cells and macrophages and inducing endothelial to mesenchymal trans-differentiation and renal fibrosis [41].

A number of studies reported that, TNF-α, interleukin (IL)-1 and IL-6 are upregulated and induce the inflammatory cascades [40]. In tubular cells albuminuria by itself stimulate the expression of IL-8 via the NF-κB/PKC pathway and ROS production [42]. Activation of PKC-β is strongly associated with glycaemic control and is responsible of different effects including the increased activity of angiotensin II, dysregulation of nitric oxide, endothelial dysfunction, and activation of MAPK and NF-κB [43]. p38 MAPK activation correlates to renal inflammation while the induction of the transcription factor NF-κB regulates the expression of various cytokines, chemokines, and adhesion molecules [44, 45].

Fibrosis

The progression of the fibrotic process, and in particular of the tubule-interstitial fibrosis, correlates with the decline in renal function and leads to ESRD [46, 47].

Renal fibrosis is a consequence of multiple cellular events including excessive proliferation and activation of fibroblasts, increased deposition of ECM, recruitment of inflammatory cells, tubular atrophy, glomerulosclerosis and microvascular rarefaction [48,49] (Figure 3).

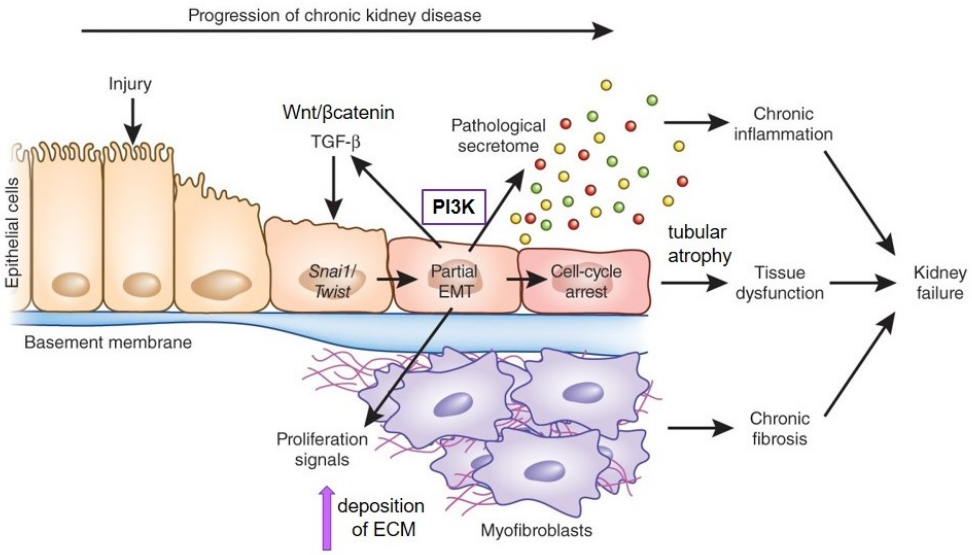

Figure 3. *Development of kidney fibrosis: overview of molecular mechanisms. [Modified from Ovadya 2015]*

In glomeruli different cell types (endothelial cells, mesangial cells, visceral epithelial cells, and parietal epithelial cells) can secrete ECM components such as type IV and type VI collagen, laminin, and fibronectin. Under pathological condition, matrix synthesis increases and matrix protein deposition inside the mesangial area reduces the capillary lumen leading to glomerular cell apoptosis [49]. Increased glucose level not only induce mesangial cell proliferation, but stimulate the secretion of pro-inflammatory citokines such as IL-1β, IL-6, TNF, CCL2/3, CXCL8 or pro-fibrotic factors (TGF-β, fibronectin). All these factors in turn activate stress-activated pathways and enhance oxidative stress level [50]. As the result of endothelial injury, capillary basement membrane is exposed and podocytes undergo damage, decreasing their filtration capacity. All of this events translate into glomerulosclerosis. Fibrosis is further sustained by the activation of interstitial fibroblasts into myofibroblasts that increase ECM secretion as response to injury [49]. Myofibroblasts can originate from different precursors including resident fibroblasts, pericytes, epithelial cells, endothelium, and circulating bone-marrow-derived cells [52]. Renal fibroblasts display several functions including ECM production, EPO and hepatocyte growth factor (HGF) secretion, and mediate the interactions with resident cells and inflammatory cells. It has been shown that the ratio of expression of the fibroblast activation protein (FAP) and α-SMA plays a role in dictating the myofibroblast phenotype. Gene expression and functional analysis demonstrated that the main function of fibroblasts expressing high levels of FAP is the synthesis and the degradation of the ECM. Meanwhile, high expression of α-SMA in myofibroblasts dictates their contraction and proliferative capacity. Local ECM composition and stiffness, as well as TGF-β signalling, appear to govern the ratio of FAP+ fibroblasts and α-SMA+ myofibroblasts [52].

Maladaptive proximal tubular injury additionally contributes to kidney fibrosis. Moreover, hyperglycaemia or AGE stimulate proximal tubular cells to secrete pro-fibrotic cytokines. It has been also demonstrated that high glucose concentration stimulates proximal tubular epithelial cells (TECs) to secrete ECM proteins via TGF-β-dependent pathway and JAK/STAT axes [53, 54]. Liu et al. have found that STAT1 underwent activation in human renal tubular epithelial cell cultured in the presence of high glucose concentration as well as in diabetic rats. STAT1 and STAT3 activation induces the expression of α-SMA and inhibits the expression of cytokeratin 18 (CK18), while overexpression of SOCS1 and SOCS3, inhibit JAK/STAT pathway and rescues these effects both in TEC and in mice [55].

Epithelial-to-mesenchymal transition (EMT) is a crucial process occurring during fibrosis and induces the activation of myofibroblasts. This translates into *de novo* deposition of ECM molecules, such as collagen I, fibronectin and laminin. TGF-β superfamily plays a pivotal role in fibrosis [56]. It regulates multiple cellular processes such as proliferation, apoptosis and

autophagy [57]. TGF-β is secreted as precursor, and maintained in its inactive form by binding to latent TGF-β binding protein (LTBP) and to the latency associated peptide (LAP). Metalloproteinase (MMP) 2, MMP9 and other proteases cleave the TGF-β latent form releasing its active form. TGF-β can exert pro-fibrotic effect through different mechanisms: (1) directly induces the ECM synthesis via Smad3- dependent or Smad3-independent manner; (2) suppresses the ECM degradation by inhibiting MMPs and inducing natural MMP inhibitors, such as tissue inhibitor of metalloproteinases (TIMPs); (3) induces transdifferentiation of several cell types toward myofibroblast via EMT, endothelial cells via endothelial–mesenchymal transition (EndMT), pericytes, and bone marrow-derived macrophages via macrophage–myofibroblast transition (MMT) [57,58]. Furthermore, TGF-β directly acts on different renal resident cells to induce mesangial cell proliferation as well as TEC, podocyte, and endothelial cell removal, leading to a more severe renal damage and fibrosis [59, 60].

The PI3K/Akt signalling pathway additionally contributes to kidney fibrosis. As TGF-β, PI3K/Akt is a multi-functional signalling cascade that mediates cell proliferation, differentiation, metabolism, and many other physiological processes [61]. In DN, PI3K/Akt signalling pathway is closely related to ECM deposition and fibrosis.

High glucose environment translates into the abnormal activation of Akt and overexpression of TGF-β both of which participate to the EMT and to the interstitial fibrosis [62]. On the contrary, the negative regulator of PI3K, PTEN reduces ECM accumulation and inhibits the secretion of the connective tissue growth factor (CTGF) easing renal damage [63]. Moreover, an additional endogenous Akt inhibitor, the Carboxyl-Terminal Modulator Protein (CTMP), was shown to reduce tubule-interstitial fibrosis by decreasing phospho-Akt, TGF-β, α-SMA activation/expression, and collagen I/II secretion [41, 64].

Recent studies have provided evidence that the Wnt/β-catenin signalling pathway is associated to progression of renal fibrosis [65]. Wnt/β-catenin pathway is involved in cell differentiation, proliferation, apoptosis and migration through downstream effectors.

It has been demonstrated that in diabetic kidney and in renal proximal tubular cells cultured in the presence of high glucose, the expression of Wnt and β-catenin was significantly increased and consistent with the increased expression of CTGF and fibronectin [66]. Moreover, increased expression of the β-catenin target genes, Snail and Twist in high glucose cultured TEC indicate the activation of the EMT. These two molecules can inhibit E-cadherin expression and increase the expression of fibronectin, αSMA and vimentin [67].

Autophagy

Autophagy is an intracellular mechanism which is activated in response to cellular stress in order to maintain tissue homeostasis. As the term suggests, autophagy is a "self-eating" process driving degradation of cytosolic proteins and organelles to provide energy to the cell [68]. Autophagy is strictly regulated all along the signalling cascade. Autophagy initiates by the formation of a double-membrane structure termed phagophore which surrounds the cytoplasmic material undergo degradation. The expansion and closure form of phagophore is the so called autophagosome. The autophagosome docks and fuses with lysosomes to form the autolysosome, in which the cytoplasmic substrates undergo degradation by acidic lysosomal hydrolases [68]. The complete autophagy dynamic flow is denoted as autophagic flux and is coordinated by 36 different autophagy-related (ATG) proteins.

Key upstream regulators of this multistep process include the highly conserved nutrient sensors mTOR and the AMP-activated kinase (AMPK) which directly phosphorylate the Unc-51-like kinase 1 (ULK1; Atg1 in yeasts), a conserved kinase initiating the phagophore formation. In particular, mTORC1 acts as a nutrient sensor and a negative regulator of autophagy. Moreover, various stress signal like hypoxia, oxidative stress, endoplamastic reticulum (ER) stress and DNA damage may induce autophagy through different signalling pathways [69]

Phagophore nucleation is dependent on the class III phosphatidylinositol 3-kinase (PtdIns3K) complex that consists of PIK3C3/VPS34 (vacuolar protein sorting 34) lipid kinase, PIK3R4/VPS15, beclin 1/BECN1 and ATG14L. This complex produces PtdIns3P at the site of the phagophore nucleation to stabilize the membrane curvature and to recruit more downstream factors for the growth of the phagophore. The recruitment of the lipidic membrane to form autophagosome is regulated by the WD-repeat phosphoinositide interacting proteins (ATG18/WIPIs), a PtdIns3P scaffold and binding protein, and by the transmembrane protein ATG9L. ATG9-containing vesicles partially control phagophore expansion by delivering membranes. Autophagosome expansion requires two ubiquitin-like conjugation systems: the ATG12 conjugation system (ATG12-ATG5-ATG16L complex) and the microtubule-associated protein light chain 3-phosphatidyl ethanolamine (MAPLC3/LC3-PE). ATG12, a ubiquitin-like protein, which is conjugated to ATG5 after activation by ATG7 and ATG10, two E1 and E2-like enzymes respectively. Then ATG12-ATG5 associates with ATG16L to form a large protein complex. The LC3 precursor (proLC3) is cleaved by the cysteine protease ATG4 to generate LC3-I. ATG7 and ATG3 (E2-like) enzymes mediate the conjugation of the phosphatidyl ethanolamine to LC3-I to form LC3-II. The ATG12-ATG5-ATG16L complex directs LC3-II into the autophagosomal membrane. Conversion of the

cytosolic LC3-I into the membrane bound LC3-II is a marker of autophagy [68, 70] (Figure 4). Hence, LC3-II is recognised by the autophagy receptor like p62/SQSTM. The p62/SQSTM recognizes the ubiquitylated proteins or organelles targeted for degradation, whereas BCL-2/adenovirus E1B 19 kDa protein-interacting protein 3 (BNIP3), recognises and degrades mitochondria through mitophagy. Subsequently, the autophagosomes fuse with lysosomes to form autolysosomes and autophagy-vesicle content can be degraded and recycled (Figure 4).

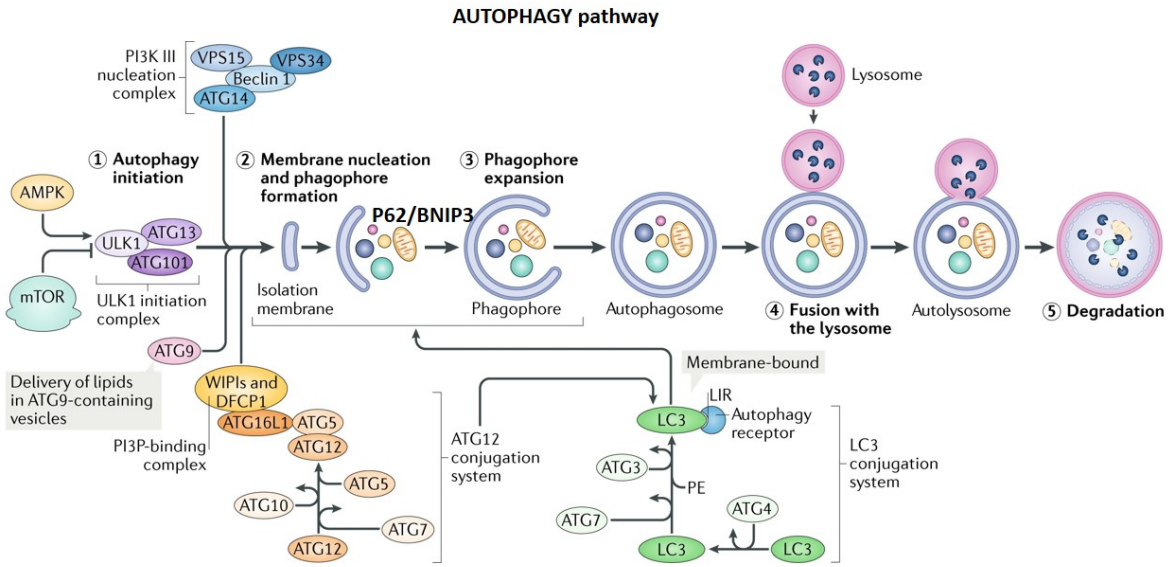

Figure 4. The autophagy cascade. *A number of autophagy-related (ATG) proteins modulated five sequential steps: 1) autophagy initiation; 2) double-membrane nucleation and formation of preautophagosome or phagophore; 3) phagophore elongation and cytoplasmic cargo sequestration; 4) fusion of the autophagosome to lysosome; and 5) degradation of the sequestered cargo in the autolysosome. mTOR, PI3K and AMPK signalling pathways are the upstream regulators of autophagy [from Hansen Nat Rev Mol Cell Biol. 2018]*

Autophagy and kidney fibrosis

Recently, several studies have demonstrated that dysregulated autophagy may contribute to the pathogenesis of renal fibrosis and its related kidney diseases [71].

In nephrotoxic and ischemic kidney injury models, autophagy is induced in proximal tubules and plays a protective role [72]. Recent works have further demonstrated the role of autophagy in fibrotic diseases involving the liver, the lung and the heart [73-75]. Moreover, depending on cells or tissues and pathological settings, autophagy can be profibrotic or antifibrotic [73, 74]. In the renal unilateral ureteral obstruction (UUO) model, autophagy occurs and induces tubular atrophy and breakdown promoting fibrosis [71, 75]. TGFβ activates autophagy in renal tubules in mice and in cultured renal tubular and mesangial cells [76]. Moreover, it has been demonstrated that autophagy may contribute to collagen I degradation and to TGFβ inactivation resulting in the inhibition of kidney fibrosis [77, 78].

Recent data have suggested that the autophagy process is abnormal in diabetic kidney disease [68]. As previously described, different upstream cellular stress sensing pathways strictly regulate autophagy. mTORC1 hyperactivation has been commonly detected in diabetic patients and in animal model of DN. In particular, mTORC1 deregulation was found associated with the altered autophagy and linked to tubular cell apoptosis and hypertrophy [79]. Two positive regulators of the autophagy flux, AMPK and Sirtuin1 (SIRT1), were also found altered in DN. AMPK activity, which is suppressed in both type 1 and 2 diabetic kidneys, could be reversed by several AMPK activators. This rescues the autophagy process and attenuates diabetic kidney injury [80]. Similar to AMPK, SIRT1 was downregulated in renal cells in humans and animal models of DN, and its activation protects the kidney from diabetes-induced injury. Mice overexpressing SIRT1 in proximal tubules were found resistant to podocyte progressive damage and subsequent proteinuria in diabetes [81]. Autophagy is also induced to maintain cell integrity by stress signalling. The loss of this adaptive response may lead to abnormal accumulation of damaged organelles, including mitochondria and ER, and has been associated to DN progression. In this regard, it has been suggested that oxidative stress via ROS and ER stress regulates autophagy in diabetic setting [82]. Moreover, in renal fibrosis the regulation of autophagy may be complex and cell-specific. In podocytes, autophagy seems to be time dependent. In fact, it was described that autophagy is induced in podocytes at week 4 after streptozotocin (STZ) injection, when mice were hyperglycemic, but still free from glomerular lesions. At week 8 post-STZ injection, along with the occurrence of glomerular lesions, autophagy undergoes inhibition in podocytes [83].

Stem cell derived extracellular vesicles and regenerative medicine

In this scenario, novel therapeutic strategies that can prevent the decline of renal function and reduce the progression of fibrosis are therefore required. Extracellular vesicles (EVs) have been proposed among the available innovative approaches.

EVs are a heterogeneous population of circular membrane fragments that are released by most cell types as exosomes and/or shedding vesicles. EVs were identified as cell-to-cell communication mechanisms that can influence the target cell by directly signal through receptor or by transfer their cargo containing several RNA species (mRNAs, miRNAs, long-non coding-RNAs, tRNAs, rRNAs, circular-RNAs and piRNAs), proteins and bioactive lipids from the cell of origin to target cell. Stem cell-derived EVs may also induce epigenetic changes in injured recipient cells with the activation of regenerative programs [84, 85] (Figure 5).

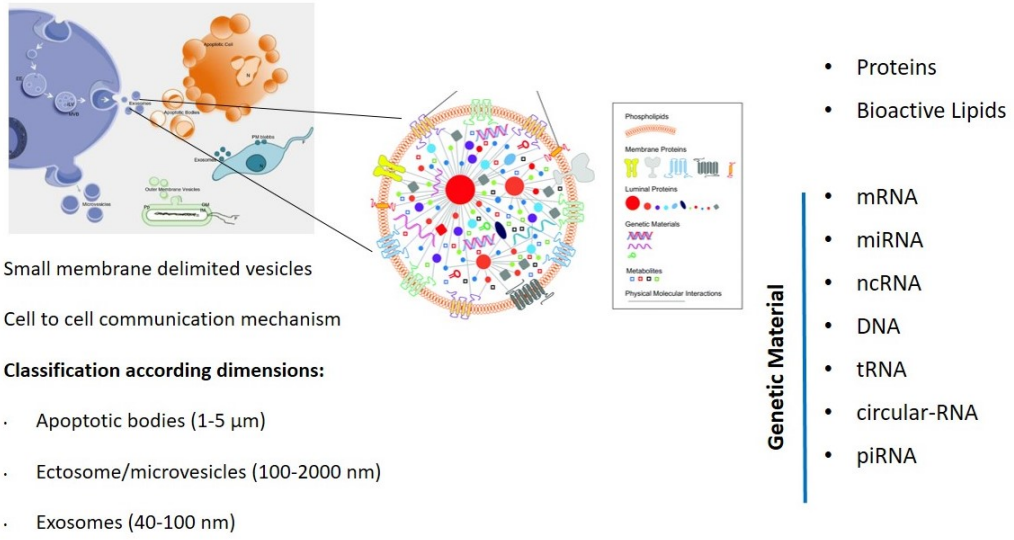

Figure 5. Extracellular vesicles overview.

In particular, EVs shed by mesenchymal stromal cells (MSC EVs) participate to cell proliferation, angiogenesis and immune escape, all of which are involved in tissue regeneration [86, 87]. Furthermore, MSC EVs from different origin (bone marrow, liver, adipose tissue, renal, cord blood and Warthon's jelly), accelerate renal repair in models of acute kidney injury (AKI) [88-90]. Multiple injections of MSC EVs also reduce the progression of renal injury in experimental models of CKD induced by five-sixth resection and unilateral ureteral obstruction [91, 92]. Kholia *et al.* have recently shown that EVs, derived from human liver stem-like cells (HLSCs) and from MSCs, significantly improve renal function and prevent fibrosis in a model of aristolochic-acid-induced CKD [93, 94]. Moreover, EVs derived from stem cells isolated from human urine and administered before the establishment of DN, were found effective in preventing kidney injury by inhibiting apoptosis in a rat model of STZ–induced diabetes [95]. The conditioned medium obtained by MSCs has also been shown to ameliorate DN progression due to the presence of paracrine factors that included exosomes. In fact, a single administration of exosomes induced a rapid improvement in renal morphology [96]. In addition to MSC-EVs, other sources of cell-derived EVs, such as endothelial colony-forming cells (ECFCs), endothelial progenitor cells (EPCs) and hypoxic TECs, have shown significant beneficial effects as well. In models of ischemic AKI, both ECFC-derived exosomes and EPC-derived EVs ameliorated renal injury via transfer of miRNAs [98, 98]. In anti-Thy1.1-induced model of glomerulonephritis, EPC-derived EVs alleviated mesangial cell activation, leukocyte infiltration and apoptosis, which was related to its content of mRNAs coding for anti-apoptotic factors and the complement inhibitors [99]. Interestingly, Dominguez et al. found that EVs derived from hypoxic TECs significantly improved renal tubular damage, fibrosis in an established renal IRI [100].

Recently, it has been demonstrated that MSCs-derived exosomes improve renal function and restore renal morphology in a rat model of STZ-induced DN. MSC EVs enhance the autophagy activity by increasing LC3 and Beclin-1, and decreasing mTOR and the expression of fibrotic markers in renal tissues. This leads to mitigation of DN progression [101]. Jin et al. have also shown that exosomes derived from adipose stem cells (ADSC EVs) attenuate DN by reducing urinary protein level, renal biochemical parameter (creatinine and Blood urea nitrogen) and podocyte apoptosis *in vivo*. ADSC EVs exert their effects by inducting autophagy and inhibiting the activation of mTOR signalling by delivering miR-486 [102].

AIM OF THE STUDY

Diabetic kidney disease is a major healthcare challenge and its complication leads to chronic kidney disease and ESRD. Several therapeutic strategies have been applied to slow down the progression of kidney disease and to reduce the cardiovascular risk, however so far effective treatment for DN and its associated complications is still an unmet need.

Hence, new therapeutics are required to ameliorate DN progression and to reduce fibrosis. Stem cell-based therapy and in particular EVs have been proposed among the available innovative approaches. The potential application of MSC EVs has attracted particular interest since EVs partly retain the biological effects of their cell of origin, without displaying the common side effects associated with cell transplantation. However so far, limited reports have described the effectiveness of human bone marrow MSC-derived EVs in preventing the progression of fibrosis and autophagy in DN.

The aim here was to deeply investigate the MSC EV mechanism of action in two different models of DN. Particular attention has been devoted to characterizing the molecular signature of MSC EV-treated kidney in order to identify potential targets. Bioinformatic analysis was also applied to discover molecules carried by MSC-EVs and potentially involved in rescuing fibrosis and regulating autophagy.

MATERIALS AND METHODS

Cell Culture

Human bone marrow Mesenchymal Stromal cells were purchased from Lonza, and were cultured in MSCBM medium supplemented with dedicated bullet kit (Lonza) and characterized as previously described [88]. Cells were used within seven passages and the characterization was performed via cytofluorimetric analysis for the expression of typical mesenchymal markers (CD44, CD105, CD73, CD90), as previously described [88]. The human lung fibroblast cell line MRC5 PD 19 (Sigma) was purchased from ATCC (Code) and cultured in DMEM supplemented with L-glutamine (5 mM), penicillin (50 IU/ml), streptomycin (50 μg/ml) (all from Sigma, St. Louis, MO, USA) and 10% heat-inactivated fetal calf serum (FCS) (EuroClone, Milan, IT).

Isolation and characterization of EVs

EVs were obtained from the supernatants of MSCs and fibroblasts (FIBRO EVs) that were cultured overnight in RPMI without FCS. After the removal of cell debris and apoptotic bodies by 3,000 g centrifugation of the supernatant for 15 minutes at room temperature of conditioned medium. EVs were purified by 2 hours of ultracentrifugation at 100,000 g and 4°C (Beckman Coulter Optima L-90K ultracentrifuge; Beckman Coulter, Fullerton, CA). EVs were resuspended in RPMI medium (EuroClone) supplemented with 1% DMSO (Sigma) and stored at -80°C. Particle size and concentration were measured using a NanoSight NS300 (NanoSight Ltd., Amesbury, UK) equipped with a 405 nm laser, and analyzed using Nanoparticle Tracking Analysis (NTA) 3.2 software. The mean EV diameter was approximately 162 ±59nm. Surface marker expression was evaluated by cytofluorimetric analysis. Approximately 1×10^9 MSC EVs were incubated with MACSPlex Exosome Capture Beads (containing 39 different antibody-coated bead subsets) and counterstained with capture beads with APC-conjugated anti-CD9, anti-CD63, and anti-CD81 antibody. Incubation was performed on an orbital shaker for 1 h at 450 rpm at room temperature in the dark. Then samples were washed in MACSPlex buffer and acquired with FACSCelesta cytofluorimeter (Beckton Dickinson). Data were analysed with BD FACSDiva 8.0.1.1 software and expressed as median fluorescence intensity (MFI) for all 39 capture bead subsets corrected by medium signal subtraction**.**

Proteomic analysis by antibody-based protein array

MSC EV protein content was analysed by human L1000 RayBiotech Protein array kit (RayBiotec, Peachtree Corners, GA, USA). MSC EVs pools from two different MSC primary

lines were lysed with 2X lysis buffer provided by the kit and following manufacturer instruction. Protein quantification was performed with BCA protein assay (Thermo Fisher). Approximately 25 µg of total protein were hybridized onto glass slide according manufacturer protocol. Fluorescence intensity was acquired, and background signal was subtract for each point. Cut-off threshold was set at 150 Fluorescent Unit (F.U.). Data are expressed as F.U. ±SD.

miRNome analysis

MSC EVs and FIBRO EVs, derived from three different preparations, were used for the extraction of RNA by a mirVana RNA isolation kit (Ambion), according to the manufacturer's protocol. miRNA content was analyzed using the qRT-PCR method and the Applied Biosystems TaqMan™ Array Human MicroRNA A+B Cards Set v3.0 (Applied Biosystems), run on QuantStudio 12K Flex (Applied Biosystems). Briefly, 140 nanograms of RNA were reverse transcribed with a Megaplex RT Pools kit (Applied Biosystems), according to the manufacturer's protocol. TaqMan® PreAmp Master Mix 2X (Applied Biosystems) and specific Megaplex™ PreAmp Primers (10X) (Applied Biosystems) were used to pre-amplify each cDNA sample, which were then loaded onto the TaqMan MicroRNA Array. Raw Ct values, the automatic baseline, threshold and comparison of miRNA expression were analyzed using Expression Suite software (Thermo Fisher Scientific, Waltham, MA). Data were matched with the MSC EV miRNA expression dataset, published in Collino *et al.* [103].

Bioinformatic analysis

miRNA target prediction was obtained from DIANAlab tool and miRwalk 3.0 [104] and pathway enrichment analysis was performed using Funrich V3.1.3 software [105]. Data with an adjusted p-value <0.05 were considered statistically significant (Hypergeometric test with Bonferroni correction). Pathway enrichment analysis for MSC EV vehicle protein was performed using Funrich V3.1.3 software and transcription factor regulated pathways and targets were analyzed with TRUUST database [106].

Mouse model of diabetic nephropathy

Animal studies were conducted in accordance with National Institute of Health Guidelines for the Care and Use of Laboratory Animals. All procedures were approved by the Ethics Committee of the University of Turin and the Italian Health Ministry (authorization number: 280/2016-PR). In preliminary setting experiments, STZ was injected in SCID and NSG mice.

We observed a more extensive kidney fibrosis development in the NSG strain than in SCID mice, so NSG strain was choosen to performed in vivo experiments (data not shown). Eight-week-old male NSG mice were purchased from the animal facility at the Molecular Biotechnology Centre. Diabetes was induced via the intraperitoneal injection of streptozotocin (37 mg/kg) that had been dissolved in freshly made in 0.1 mol/l citrate buffer, at pH 4.5, for 4 consecutive days in order to avoid acute STZ toxicity, according to Animal Models of Diabetic Complications Consortium guidelines (available at http://www.amdcc.org) [107].

Blood glucose levels were measured, after 4 hours of fasting, in blood from the tail-vein using a blood glucometer (GlucoMen LX Plus+, A. Menarini diagnostics, Florence, IT). The onset of diabetes was established by measuring glycaemia (up to 250 mg/ml) 10 days after STZ injection (T0). Glycaemia was monitored every 2 weeks and body weight and water up-take every week.

Experiments were performed according two setting (Figure 6 and 15) the preventive and the curative settings.

In the preventive setting after day 10 of STZ injection, mice were i.v. injected with $1x10^{10}$ MSC EVs each injection, once a week from day 0 (T0) for 4 weeks (T28) (5 injections) or with vehicle (CTL). In the curative setting after one month of diabetes, mice were randomly divided into MSC EV or FIBRO EV treated group and CTL DN group. EVs were injected intravenously with $1x10^{10}$ particles each injection, once a week from day 30 (T30) for 4 weeks (5 injections) whereas CTL group was injected with an equal volume of saline solution. Mice were sacrificed 28 or 60 days post diabetes. At either day 60 (T60) or day 28 (T28), urine (12 hours collection in metabolic cage) and blood were collected for the evaluation of albuminuria, creatinuria, plasma creatinine and BUN. Kidneys were collected for histology and molecular analyses.

Biochemical and histological analyses

Urine samples were collected overnight on the day prior to sacrifice and albuminuria concentration was determined using an Albumin Mouse ELISA Kit (Abcam, Cambridge, UK) according to the manufacturer's protocols. The urinary albumin results were normalized to urinary creatinine levels, which were determined using a colorimetric assay that was based on the Jaffé method (QuantiChrom Creatinine Assay Kit, BioAssay System, Hayward, USA), and were expressed as ACR.

Plasma was used to measure creatinine concentration, using a Creatinine Assay kit (Abcam), while Blood Urea nitrogen (BUN) was measured using a Urea Nitrogen Colorimetric Detection kit (Arbor Assays, Michigan, USA) according to the manufacturers' protocols.

Renal tissues were embedded in paraffin and 5 μm sections were stained with hematoxylin and eosin staining, as well as PAS and Masson's Trichrome staining (Bio-Optica, Milan, IT) according to the manufacturer's protocols. Interstitial and glomerular fibrosis were quantified in Masson's Trichrome stained sections, using ImageJ software, calculated from 10 random cortical pictures per section at 200X magnification, and expressed as mean values ±SEM [108]. Glomerular injury was determined by measuring glomerular area and Bowman's space using ImageJ software on 15 glomeruli from each mouse that were stained with PAS (magnification: 400X) [109]. The number of injured tubules in 10 random images per cortical section was counted using 200X magnification with hematoxylin and eosin staining.

Immunofluorescence

Paraffin renal tissue sections were deparaffinized in xilol and rehydratated in ethanol bath at different percentage. Antigen retrieval was obtained by boiling slides 15 minutes in citrate buffer and cool for other 15 minutes. Tissue specimens were then blocked in PBS 1X+5% Bovine Serum Albumin (BSA) + 0.1% Triton-X-100 (Sigma). Tissues were incubated with specific primary antibody anti-LC3B (Sigma, L7543). After washing with PBS 1X+0.1% BSA, slides were incubated with specific anti rabbit- TexasRED secondary antibody (1:1,000 Invitrogen). Hoechst was used for nuclear staining. Section were mount with Fluormount mounting medium (Sigma) and acquired with Apotome Zeiss microscope at 400X magnification (Zeiss). Five mice per group and 6 images per mice were analyzed with ImageJ software to count LC3 positive dots.

TUNEL

TUNEL assay (ApopTagOncor, Gaithersburg, MD) was performed accordingly manufacture's protocol. Number of TUNEL-positive cells were evaluated by counting the number of positive nuclei per field in 10 randomly chosen sections using ImageJ software.

Transcriptomic analysis of kidney tissue

PCR arrays

The kidneys of healthy (n=3), diabetic CTL (n=3), MSC EV (n=3) and FIBRO EV (n=3)-treated mice at day 28 and day 30 were homogenized in a Bullet blender (Next Advance Inc, NY, USA) at a speed of 8 rpm for 3 minutes using 3.2 mm size zirconium pellets. RNA was extracted by Trizol (Ambion, Austin, TX, USA), according manufacturer's instructions, and quantified on a Nanodrop ND-2000 (Nanodrop, Wilmington, DE, USA) spectrophotometer. Four hundred nanograms of RNA were retrotranscribed for each sample using a RT^2 First

Strand kit (Qiagen, Frederick, MD, USA) according the manufacturer's instructions. cDNA was run using a RT² Profiler™ PCR Array Mouse Fibrosis- PAMM-120Z **(**Qiagen) or RT² Profiler™ PCR Array Mouse Autophagy PAMM-84Z on a StepOne PlusTM System (Applied Biosystems, Foster City, CA, USA). Data analysis was conducted using Expression Suite software (Applied Biosystems) with appropriate threshold and baseline values. The Ct cut-off was set at <35. Differential expression analysis was performed using Qiagen on-line software and by comparing the expression of all groups versus CTL mice and versus healthy mice. We selected and considered the geometric mean of housekeeping genes with low variability for normalization from among the different samples. Relative quantification (RQ) was calculated using the ΔΔCt method. Genes with RQ <0.6 were considered to be downregulated (green) and ones with RQ >1.8 were considered to be upregulated (red). p values were calculated using a Student's t-test of the replicate $2^{-\Delta Ct}$ values for each gene in the control and treatment groups, and was set at <0.05 (light blue).

Real time PCR

The expression of pro-fibrotic markers (α-SMA, Collagen I and TGF-β) and the expression of autophagy related genes was evaluated using qRT-PCR. cDNA was obtained using a High Capacity cDNA reverse transcription kit (Applied Biosystems) and PCR reactions were carried out using a Power SYBR Green PCR Master Mix (Applied Biosystems) and the specific set of primers listed in Table 1. Mouse GAPDH or βActin were used as endogenous control gene. Data were analyzed according to the ΔΔCt method.

Gene symbol	Forward	Reverse
m_Col1	ATCTCCTGGTGCTGATGGAC	ACCTTGTTTGCCAGGTTCAC
m_Tgfb1	CGAAAGCCCTGTATTCCGTCT	GCAACAATTCCTGGCGTTACC
m_α-Sma	CTGACAGAGGCACCACTGAA	CATCTCCAGAGTCCAGCACA
m_Gapdh	TGTCAAGCTCATTTCTGGTATGA	TCTTACTCCTTGGAGGCCATGT
m_Ambra	CAGTGAGAACAACTCCAACCTGTCT	TTTCCCAACGAAGGGTATCATT
m_Akt1	TCCACGCTCCTCTGCATTG	CCAGCGCATCCGAGAAAC
m_Atg7	AGCAGTGATGACCGCATGAA	TGACAGAAAACCCCGGATCTG
m_Atg9b	TCCTTCGCTGCGTGGATTAC	TGGCATCTGACAAGGTCACTTT
m_Wipi	GGAGACCGTGCACATCTTCA	GCTCCAGGTGGAAGGCTCTT
m_Sqstm1	TGTGGAACATGGAGGGAAGAG	TTCTGTGCCTGTGCTGGAACTT
m_Beclin1	CTGGCACAGCGGACAGTTT	TCATTCCACTCCACAGGAACACT
m_βActin	GATTACTGCTCTGGCTCCTAGCA	GCCACCGATCCACACAGAGT

Table 1. PCR primer set

Western blot

Kidney tissue were lysed in RIPA lysis buffer supplemented with protease/fosfatase inhibitors (Sigma Aldrich) for 15 minutes at 4°C and centrifuged at 12,000 g. Supernatants were collected and quantified by Bradford method (Biorad). Western blot analyses were performed using 10% SDS-PAGE electrophoresis gel (Biorad) and blotted with an iBLOT device (Invitrogen) onto nitrocellulose membrane filters. The following primary antibodies were used: LC3 (Sigma, L7543), p62 (CST, D5L7G).

Statistical analysis

Statistical analyses were performed using Graph Pad Prism version 5.04 (Graph Pad Software, Inc, La Jolla, CA, USA). Comparisons between groups were either analyzed using a Student's t-test or by ANOVA, followed by the Dunnet's multi comparison test, when appropriate. A p value of < 0.05 was considered significant.

RESULTS

MSC EV morphology and surface marker characterization

MSC EVs were characterized by NTA and mean EV diameter was approximately 162 ±59nm (Figure 1). MSC EVs express the typical mesenchymal and exosomal markers as shown by MACS PLEX analysis.

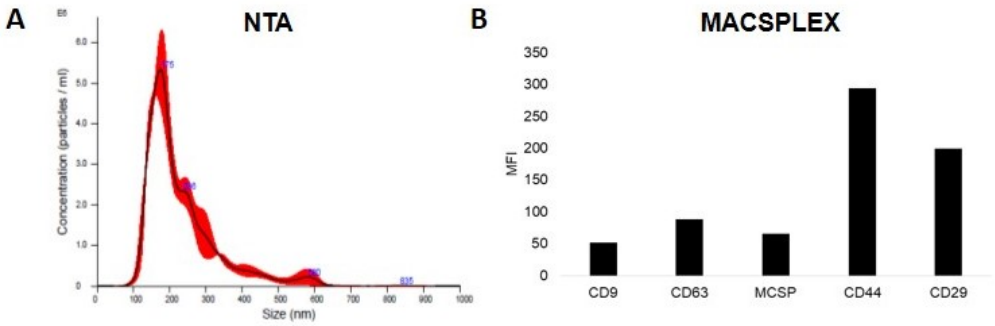

Figure 1. MSC EV characterization *A) Representative NTA analysis on MSC EVs. B) Cytofluorimetric analysis of surface markers by MACSPlex.*

MSC EV protein cargo

EV protein samples were analyzed using a semi-quantitative method of antibody based protein array. The analysis allowed the simultaneous evaluation of more than 1000 proteins including cytokines, chemokines, adipokines, growth factors, angiogenic factors, proteases, soluble receptors and soluble adhesion molecules. We identified 676 proteins expressed in MSC EVs (Table 1).

Table 1. MSC EV proteins

MSC EV	Gene name	MEDIA	SD	MSC EV	Gene name	MEDIA	SD
ApoC3	APOC3	58987	8753	IL-2 R gamma	IL2RG	359	102
HRG-alpha	HRG	46949	17507	C2	C2	355	29
CD74	CD74	8740	12172	CD30 / TNFRSF8	TNFRSF8	354	72
LAG-3	LAG3	1666	200	Angiopoietin-1	ANGPT1	352	240
IL-13	IL13	706	60	VDUP-1	TXNIP	348	30
IL-21	IL21	679	74	Thrombospondin-2	THBS2	347	106
HGFR	MET	674	92	NPTX1	NPTX1	346	68
Amylin	IAPP	661	101	Insulin R	INSR	341	39
GDF11	GDF11	638	53	Ubiquitin+1	UBB	339	43
TNF-alpha	TNF	630	191	Factor XIII A	F13A1	338	159
MSHa	MSX1	629	195	IL-9	IL9	334	83
GRO	CXCL2	607	100	MIG	CXCL9	330	112
GDF3	GDF3	598	49	MIP-1b	CCL4	329	123
IFN-gamma	IFNG	592	81	IL-1 R6 / IL-1 Rrp2	IL1RL2	328	35
BD-1	DEFB1	582	118	PDGF R beta	PDGFRB	326	50
IL-7	IL7	580	112	Clusterin	CLU	323	84

MSC EV	Gene name	MEDIA	SD	MSC EV	Gene name	MEDIA	SD
IL-6	IL6	568	132	BMP-7	BMP7	321	12
GDF9	GDF9	550	55	S100 A8/A9	S100A8	317	97
Granzyme A	GZMA	546	78	LH	LHCGR	308	69
GDF5	GDF5	543	73	PARC / CCL18	CCL18	307	66
GDF8	MSTN	531	102	ENPP2	ENPP2	306	44
TNF-beta	LTA	506	112	IL-10 R alpha	IL10RA	303	55
TGF-beta 1	TGFB1	502	43	CA 19-9	MUC16	298	70
IL-1 alpha	IL1A	499	70	MIP 2	CXCL2	298	80
IL-2	IL2	492	68	IL-1 sRI	IL1R1	296	67
IL-5	IL5	490	86	P-selectin	SELP	296	15
MIP-3 beta	CCL19	485	164	TXK	TXK	295	53
IL-8	CXCL8	483	72	TRAIL R1 / DR4 / TNFRSF10A	TNFRSF10A	295	67
BAI-1	ADGRB1	479	122	MMP-20	MMP20	294	4
Mammaglobin A	SCGB2A2	464	32	HCR / CRAM-A/B	CCHCR1	293	28
CNTF R alpha	CNTFR	425	24	Alpha Lactalbumin	LALBA	291	49
CNTF	CNTF	422	77	GITR Ligand / TNFSF18	TNFSF18	291	62
IL-15	IL15	416	81	SERPING1	SERPING1	288	79
GDF1	GDF1	416	32	CCL28 / VIC	CCL28	283	15
Erythropoietin	EPX	412	64	Ceruloplasmin	CP	283	89
GREMLIN	GREM1	400	69	CTACK / CCL27	CCL27	282	46
Growth Hormone (GH)	GH1	390	78	MCP-1	CCL2	281	80
IL-2 R beta /CD122	IL2RB	387	35	TRAIL R2 / DR5 / TNFRSF10B	TNFRSF10B	280	63
GFR alpha-3	GFRA3	382	40	SAA	SAA1	280	99
EDG-1	S1PR1	372	86	Glut5	SLC2A5	280	51
CD71	TFRC	371	55	TRA-1-81	PODXL	278	42
Aldolase C	ALDOC	278	61	CD 163	CD163	235	127
XEDAR	EDA2R	277	35	Hepassocin	FGL1	234	31
L-Selectin (CD62L)	SELL	276	63	Ntn1	NTN1	234	80
ALPP	ALPP	275	15	CTLA-4 /CD152	CTLA4	232	34
Tec	TEC	272	34	Angiopoietin-like 1	ANGPTL1	231	40
ACK1	TNK2	272	21	C-peptide	INS	230	36
Frizzled-1	FZD1	271	54	Chordin-Like 2	CHRDL2	230	56
Follistatin	FST	270	34	Siglec-9	SIGLEC9	229	73
FGF-10 / KGF-2	FGF10	270	47	Calcitonin	CALCA	227	7
TGF-beta 5	TGFB5	270	68	ALCAM	ALCAM	226	263
TRA-1-60	PODXL	269	16	GM-CSF R alpha	CSF2RA	225	21
IL-1 R4 / ST2	IL1RL1	269	53	Itk	ITK	225	50
GCSF	CSF3	266	87	Corticosteroid-binding globulin	SERPINA6	225	47
Troponin C	TNNC1	265	26	Sonic Hedgehog (Shh N-terminal)	SHH	223	47
FER	FER	264	95	IL-1 F10 / IL-1HY2	IL1F10	223	71
IL-11	IL11	263	39	SHBG	SHBG	223	59
Aldolase A	ALDOA	261	46	Musk	MUSK	222	59

MSC EV	Gene name	MEDIA	SD
MSP alpha Chain	MST1	259	63
SDF-1 / CXCL12	CXCL12	258	94
IL-20 R alpha	IL20RA	258	57
IL-13 R alpha 1	IL13RA1	257	83
IL-17	IL17A	256	62
Dkk-4	DKK4	256	32
MINA	RIOX2	255	87
Btk	BTK	251	18
BNP	NPPB	250	29
FGF-16	FGF16	250	50
CHI3L1	CHI3L1	249	57
ApoA4	APOA4	248	32
MMP-8	MMP8	247	21
Creatinine	CSH1	246	17
A1BG	A1BG	246	42
AgRP	AGRP	245	30
Cytokeratin 19	KRT19	244	40
Lyn	LYN	244	25
NRG3	NRG3	243	47
CPN2	CPN2	242	54
Cryptic	CFC1	241	55
GASP-2 / WFIKKN	WFIKKN1	239	96
SLPI	SLPI	238	64
EphA4	EPHA4	235	2
FRK	FRK	197	39
GFR alpha-4	GFRA4	197	52
Fibrinopeptide A	FGA	195	38
Angiostatin	PLG	193	49
FGF-20	FGF20	193	51
Kallikrein 2	KLK2	193	31
FGF-11	FGF11	193	28
ASPH	ASPH	192	60
PPARg2	PPARG	191	16
PDGF R alpha	PDGFRA	190	45
GASP-1 / WFIKKNRP	WFIKKN2	189	102
Kremen-1	KREMEN1	189	15
APC	APC	189	21
EMAP-II	EML2	188	46
IL-23p19	IL23A	188	32
TPX	TPO	186	15
ZAP70	ZAP70	220	10
CV-2	BMPER	220	46

MSC EV	Gene name	MEDIA	SD
Glut1	SLC2A1	220	26
MAC-1	ITGAM	219	102
FGF-5	FGF5	217	66
Glut2	SLC2A2	215	56
BMP-5	BMP5	214	53
Siglec-5/CD170	SIGLEC5	214	55
Galanin	GAL	213	48
FGF-18	FGF18	212	66
NR3C3	PGR	211	37
LRG1	LRG1	210	68
FGF-17	FGF17	210	30
Endoglin / CD105	ENG	209	58
BTC	BTC	209	39
MATK	MATK	209	16
Lck	LCK	207	83
Legumain	LGMN	206	58
INSRR	INSRR	204	156
PI 3Kinase p85 beta	PIK3R1	204	8
IL-1 R8	IL1RAPL1	203	59
BNIP2	BNIP2	202	37
TACI / TNFRSF13B	TNFRSF13B	200	3
Fyn	FYN	200	34
Frizzled-3	FZD3	168	22
TYRO10	DDR2	167	14
Thrombospondin-1	THBS1	166	101
A2M	A2M	165	47
TRADD	TRADD	165	51
CCL14 / HCC-1 / HCC-3	CCL14	164	26
NOV / CCN3	NOV	163	35
FGF-13 1B	FGF13	163	38
MMP-24 / MT5-MMP	MMP24	163	32
Bax	BAX	163	54
IL-1 sRII	IL1R2	162	24
Galectin-3	LGALS3	162	4
Tarc	CCL17	162	71
GITR / TNFRF18	TNFRSF18	162	40
HSP27	HSPB1	162	2
IL-17RC	IL17RC	162	11
MMP-2	MMP2	185	25
GMNN	GMNN	184	87
BMP-8	BMP8B	184	32
PEPSINOGEN I	PGC	183	12

MSC EV	Gene name	MEDIA	SD
E-Selectin	SELE	182	35
Progesterone	Progesterone	181	19
CK-MB	CKB	181	43
GLP-1	ZGLP1	181	12
CBP	CREBBP	180	10
Vasorin	VASN	179	55
IL-10	IL10	179	83
ADAMTS-17	ADAMTS17	178	10
VGF	VGF	176	28
Thymopoietin	TMPO	175	73
GM-CSF	CSF2	174	56
IL-17B R	IL17RB	174	13
ADAMTS-4	ADAMTS4	174	27
GADD45A	GADD45A	174	40
Fibronectin	FN1	173	100
RELT / TNFRSF19L	RELT	173	58
ACTH	POMC	173	16
LPS	IRF6	171	56
LTF	LTF	171	88
CLC	CLC	170	28
EV15L	EVI5L	169	35
ABL1	ABL1	161	2
Calbindin	CALB1	161	28
TSH	TSHB	161	38
Orexin B	HCRTR2	158	34
Netrin G2	NTNG2	158	34
FOXN3	FOXN3	157	3
GRP	GRP	155	19
Mesothelin	MSLN	154	200
MMP-19	MMP19	154	88
FGFR1 alpha	FGFR1	153	13
Haptoglobin	HP	152	27
AFP	AFP	151	21
ANGPTL3	ANGPTL3	151	67
FGF R5	FGFRL1	150	65
NRG2	NRG2	150	5

Table 1. List of proteins vehicle by MSC-EVs expressed as Fluorescence Intensity ± SD

Pathway enrichment analysis showed that most of them are mainly related to signal transduction, cell communication, and immune response. Moreover, we observed that discrete

proteins are involved in DN-related pathways. They include PI3K-mTOR, VEGF, and PDGF (Figure 2).

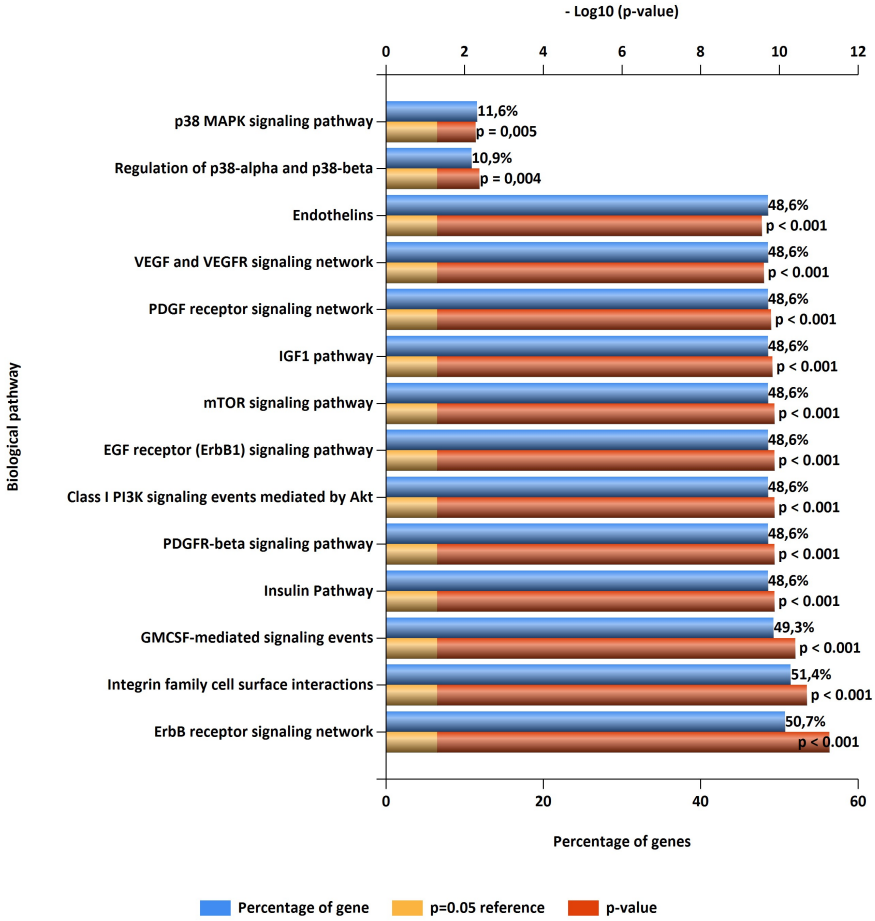

Figure 2. Pathway enrichment analysis of proteins vehciled by MSC EVs

MSC-EV miRNA cargo analysis

miRNA content of MSC-EVs was screened by Taqman microfluidic PCR array and was compared with FIBRO EV miRNAs used as internal negative control. 211 miRNAs were detected in MSC EVs (Table 2) while 59 were specifically expressed in MSC EVs compared to FIBRO EVs (Table 3 and Figure 3A).

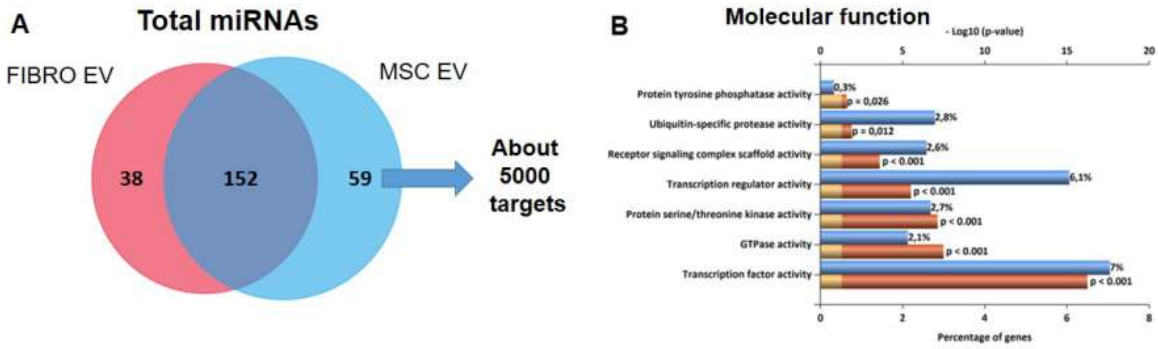

Figure 3. Screening of miRNA cargo of MSC EVs and FIBRO EVs. *A) Venn dagram showing miRNA commonly or specificcaly vehicle by MSC EVs and FIBRO EVs; B) Gene Ontology analysis of molecular function category of MSC EV specific miRNA-targets.*

For target prediction analysis only miRNAs expressed in MSC EVs, but not in FIBRO EV were considered. In MSC EVs around 5000 genes were predicted as miRNA targets. Gene ontology analysis indicates that these targets are mainly involved in transcription activity and transcription regulation, protein serine/threonine kinase activity and transporter activity (Figure 3B).

Table 2. MSC EV miRNAs

miRNA name	CT mean	SD
hsa-miR-222-3p	21.58	2.24
hsa-miR-24-3p	21.64	1.65
hsa-miR-302c-3p	21.87	7.23
hsa-miR-99a-5p	22.90	1.65
hsa-let-7b-5p	22.93	1.20
hsa-miR-1243	23.31	12.71
hsa-miR-100-5p	23.35	1.87
hsa-let-7e-5p	23.84	2.50
hsa-miR-191-5p	23.87	1.91
hsa-miR-125b-5p	24.08	2.06
hsa-miR-21-5p	24.15	2.85
hsa-miR-193b-3p	24.23	1.73
hsa-miR-31-5p	24.25	2.00
hsa-miR-30a-5p	24.28	3.07
hsa-miR-574-3p	24.33	1.80
hsa-miR-145-5p	24.42	2.49
hsa-miR-214-3p	24.45	1.63
hsa-miR-320a	24.65	1.67
hsa-miR-1260a	24.94	3.15
hsa-miR-197-3p	25.03	2.44
hsa-miR-30a-3p	25.04	2.55
hsa-miR-199a-3p hsa-miR-199b-3p	25.08	1.69
hsa-miR-374b-5p	25.09	2.41
hsa-miR-484	25.25	1.80
hsa-miR-221-3p	25.26	2.22
hsa-miR-409-3p	25.31	3.21
hsa-miR-186-5p	25.40	1.83
hsa-miR-30c-5p	25.42	2.10
hsa-miR-29a-3p	25.47	1.92
hsa-miR-138-5p	25.48	2.59
hsa-miR-99b-5p	25.70	1.50
hsa-miR-16-5p	25.71	1.83
hsa-miR-106a-5p	25.89	1.74
hsa-miR-888-5p	25.91	7.82
hsa-miR-17-5p	25.92	1.40

miRNA name	CT mean	SD
hsa-miR-19b-3p	26.03	1.72
hsa-miR-30b-5p	26.27	2.00
hsa-miR-26a-5p	26.39	1.70
hsa-miR-31-3p	26.49	1.78
hsa-miR-30e-3p	26.65	2.22
hsa-miR-125a-5p	26.77	1.89
hsa-miR-331-3p	26.81	2.08
hsa-miR-1270	26.88	2.43
hsa-miR-140-5p	27.06	1.89
hsa-miR-20a-5p	27.07	2.33
hsa-miR-149-5p	27.16	2.24
hsa-miR-376c-3p	27.27	2.40
hsa-miR-204-5p	27.33	3.62
hsa-miR-34a-5p	27.36	2.08
hsa-miR-152-3p	27.38	1.35
hsa-miR-193a-5p	27.49	2.23
hsa-miR-328-3p	27.55	1.38
hsa-miR-1275	27.61	3.10
hsa-miR-181a-5p	27.73	1.99
hsa-let-7d-5p	27.77	1.82
hsa-miR-126-5p	27.79	0.96
hsa-miR-25-3p	27.83	2.20
hsa-miR-143-3p	27.88	2.43
hsa-miR-92a-3p	27.89	2.39
hsa-miR-425-5p	27.94	1.03
hsa-miR-382-5p	28.19	3.60
hsa-miR-365a-3p hsa-miR-365b-3p	28.21	2.01
hsa-let-7g-5p	28.22	1.70
hsa-miR-342-3p	28.30	1.53
hsa-miR-28-3p	28.30	2.08
hsa-miR-376a-3p	28.33	2.04
hsa-miR-370-3p	28.36	2.46
hsa-miR-146b-5p	28.36	1.45
hsa-miR-150-5p	28.56	1.50
hsa-miR-133a-3p	28.69	2.68

miRNA name	CT mean	SD
hsa-miR-93-5p	28.79	1.42
hsa-miR-638	28.85	2.13
hsa-miR-532-5p	28.85	2.67
hsa-miR-485-3p	28.88	1.67
hsa-miR-132-3p	28.98	4.22
hsa-miR-539-5p	29.02	2.01
hsa-miR-10a-5p	29.10	1.31
hsa-miR-483-5p	29.13	2.15
hsa-miR-411-5p	29.15	1.88
hsa-miR-34a-3p	29.15	2.01
hsa-miR-374a-5p	29.24	2.11
hsa-miR-432-5p	29.26	3.00
hsa-miR-335-5p	29.33	1.80
hsa-miR-195-5p	29.34	1.81
hsa-miR-494-3p	29.35	1.98
hsa-miR-27a-3p	29.44	3.97
hsa-miR-495-3p	29.49	1.32
hsa-miR-218-5p	29.52	2.06
hsa-miR-134-5p	29.55	2.86
hsa-miR-345-5p	29.56	1.30
hsa-miR-10b-3p	29.58	2.08
hsa-miR-625-3p	29.65	1.62
hsa-miR-27b-3p	29.69	2.41
hsa-miR-335-3p	29.70	3.87
hsa-miR-486-5p	29.73	1.71
hsa-miR-339-3p	29.77	3.39
hsa-miR-210-3p	29.78	6.83
hsa-miR-193b-5p	29.80	1.28
hsa-miR-590-5p	29.85	2.56
hsa-miR-34b-3p	29.90	1.05
hsa-miR-744-5p	29.90	1.63
hsa-let-7c-5p	29.92	2.45
hsa-miR-454-3p	29.95	1.91
hsa-miR-379-5p	29.99	1.43
hsa-miR-769-5p	30.05	1.76

miRNA name	CT mean	SD
hsa-miR-323a-3p	30.06	2.13
hsa-miR-19a-3p	30.06	2.00
hsa-miR-137	30.12	2.23
hsa-miR-320b	30.13	2.29
hsa-miR-106b-5p	30.14	1.97
hsa-miR-224-5p	30.14	1.81
hsa-miR-222-5p	30.18	3.38
hsa-miR-20b-5p	30.30	1.79
hsa-miR-196b-5p	30.30	2.45
hsa-miR-29a-5p	30.33	3.07
hsa-miR-130a-3p	30.73	1.99
hsa-miR-136-3p	30.76	2.50
hsa-miR-1233-3p	30.77	6.22
hsa-miR-130b-3p	30.83	2.36
hsa-miR-26b-5p	30.93	2.60
hsa-miR-103a-3p	30.95	3.74
hsa-miR-151a-3p	30.99	3.15
hsa-miR-203a-3p	31.02	0.73
hsa-miR-202-3p	31.03	0.93
hsa-let-7a-5p	31.03	6.57
hsa-miR-214-5p	31.08	3.04
hsa-miR-99b-3p	31.11	0.77
hsa-miR-423-5p	31.11	1.54
hsa-miR-377-3p	31.12	10.28
hsa-miR-708-5p	31.18	3.96
hsa-miR-22-5p	31.33	4.42
hsa-miR-146a-5p	31.33	3.01
hsa-miR-493-3p	31.35	1.46
hsa-miR-324-3p	31.39	2.08
hsa-miR-452-5p	31.39	1.91
hsa-miR-1291	31.42	1.98
hsa-miR-636	31.44	3.49
hsa-miR-15b-5p	31.46	2.59
hsa-miR-543	31.47	3.49
hsa-miR-33a-3p	31.47	1.96
hsa-miR-155-5p	31.50	1.02
hsa-miR-30d-5p	31.51	3.18
hsa-miR-487b-3p	31.55	1.56
hsa-miR-129-2-3p	31.70	1.70
hsa-miR-885-5p	31.74	5.79
hsa-miR-664a-3p	31.84	1.76

miRNA name	CT mean	SD
hsa-miR-1208	31.84	3.29
hsa-miR-28-5p	31.87	5.43
hsa-miR-483-3p	31.89	5.59
hsa-miR-433-3p	31.93	5.39
hsa-miR-410-3p	31.94	1.53
hsa-miR-1271-5p	31.96	3.61
hsa-miR-601	31.96	1.96
hsa-miR-503-5p	31.97	5.63
hsa-miR-29b-3p	32.01	2.39
hsa-miR-184	32.09	5.32
hsa-miR-151a-5p	32.13	3.50
hsa-miR-1290	32.13	5.35
hsa-miR-572	32.22	2.53
hsa-miR-367-3p	32.24	9.07
hsa-miR-212-3p	32.33	5.17
hsa-miR-93-3p	32.33	5.23
hsa-miR-215-5p	32.35	2.73
hsa-miR-27a-5p	32.42	1.19
hsa-miR-223-3p	32.50	2.71
hsa-miR-505-3p	32.58	5.07
hsa-miR-142-3p	32.59	2.68
hsa-miR-296-5p	32.63	4.94
hsa-miR-532-3p	32.64	4.95
hsa-miR-770-5p	32.66	5.08
hsa-miR-10b-5p	32.72	5.97
hsa-miR-145-3p	32.75	2.59
hsa-miR-199a-5p	32.79	4.81
hsa-miR-324-5p	32.79	4.93
hsa-miR-660-5p	32.80	5.38
hsa-miR-140-3p	32.82	3.68
hsa-miR-338-5P	32.88	3.17
hsa-miR-200c-3p	32.88	1.70
hsa-miR-889-3p	32.91	1.44
hsa-miR-339-5p	33.00	4.89
hsa-miR-655-3p	33.03	4.70
hsa-miR-29c-3p	33.03	1.71
hsa-miR-1244	33.05	0.89
hsa-miR-21-3p	33.05	5.04
hsa-miR-125b-1-3p	33.22	3.58
hsa-miR-181a-3p	33.27	4.57
hsa-miR-301a-3p	33.37	4.43

miRNA name	CT mean	SD
hsa-miR-18a-5p	33.42	4.77
hsa-miR-1282	33.47	2.25
hsa-miR-148b-3p	33.48	4.49
hsa-miR-766-3p	33.54	4.35
hsa-miR-181a-2-3p	33.56	4.34
hsa-miR-451a	33.60	4.32
hsa-miR-194-5p	33.62	4.88
hsa-miR-362-5p	33.63	4.39
hsa-miR-671-3p	33.74	4.66
hsa-miR-500a-5p	33.79	4.44
hsa-miR-124-3p	33.82	4.19
hsa-miR-7-1-3p	33.84	2.57
hsa-miR-502-5p	33.85	4.14
hsa-miR-199b-5p	33.94	4.31
hsa-miR-548c-3p	33.95	1.12
hsa-miR-148a-3p	33.97	4.67
hsa-miR-424-3p	34.00	4.57
hsa-miR-27b-5p	34.22	4.32
hsa-miR-505-5p	34.26	2.53
hsa-miR-376b-3p	34.28	6.71
hsa-miR-425-3p	34.44	4.10
hsa-miR-628-5p	34.49	3.73

Table 2. List of miRNAs carried by MSC EVs. *Data are displayed as CT mean value ± SD (n=3). The 15 most expressed miRNAs, used in bioinformatics analysis, are highlighted in bold.*

Table 3. FIBRO EV miRNAs

miRNA name	CT mean	SD
hsa-miR-24-3p	23.12	0.24
hsa-miR-484	24.18	0.30
hsa-miR-222-3p	24.33	0.24
hsa-miR-1233-3p	24.62	0.29
hsa-miR-574-3p	24.68	0.64
hsa-miR-409-3p	24.84	1.06
hsa-miR-1247-5p	24.93	0.71
hsa-miR-191-5p	24.97	0.43
hsa-miR-320a	25.23	0.02
hsa-miR-29a-3p	25.37	0.05
hsa-miR-193b-3p	25.74	0.75
hsa-miR-31-5p	26.17	0.57
hsa-miR-19b-3p	26.19	0.03
hsa-miR-376a-3p	26.25	0.95
hsa-miR-16-5p	26.27	0.90
hsa-miR-596	26.27	0.45
hsa-miR-376c-3p	26.31	0.25
hsa-miR-1260a	26.51	1.79
hsa-miR-1225-3p	26.51	1.17
hsa-miR-197-3p	26.54	0.30
hsa-miR-214-3p	26.78	0.87
hsa-miR-149-5p	26.96	1.39
hsa-miR-155-5p	26.99	0.40
hsa-miR-571	27.03	0.08
hsa-miR-17-5p	27.04	0.06
hsa-miR-1825	27.15	0.44
hsa-miR-106a-5p	27.31	0.01
hsa-miR-370-3p	27.33	0.72
hsa-let-7b-5p	27.34	0.35
hsa-let-7e-5p	27.36	0.14
hsa-miR-99a-5p	27.39	0.90
hsa-miR-199a-3p hsa-miR-199b-3p	27.42	1.18
hsa-miR-146a-5p	27.51	0.06
hsa-miR-1267	27.54	6.38
hsa-miR-432-5p	27.60	0.28
hsa-miR-663b	27.72	0.81
hsa-let-7b-3p	27.75	1.07
hsa-miR-134-5p	27.95	0.15
hsa-miR-454-3p	27.97	0.56
hsa-miR-100-5p	28.00	0.10
hsa-miR-331-3p	28.04	0.41

miRNA name	CT mean	SD
hsa-miR-186-5p	28.05	0.01
hsa-miR-374b-5p	28.26	0.06
hsa-miR-30a-3p	28.30	0.60
hsa-miR-21-5p	28.41	0.01
hsa-miR-342-3p	28.41	0.62
hsa-miR-345-5p	28.52	0.19
hsa-miR-30e-3p	28.56	0.28
hsa-miR-138-5p	28.64	0.39
hsa-miR-1227-3p	28.64	0.58
hsa-miR-30c-5p	28.79	0.07
hsa-miR-411-5p	28.84	0.20
hsa-miR-221-3p	28.87	0.60
hsa-miR-145-5p	28.98	0.17
hsa-miR-125a-5p	28.98	0.18
hsa-miR-28-3p	28.99	0.25
hsa-miR-146b-5p	29.03	0.94
hsa-miR-34b-3p	29.07	0.84
hsa-miR-222-5p	29.08	0.86
hsa-miR-770-5p	29.11	0.98
hsa-miR-20a-5p	29.12	0.42
hsa-miR-26a-5p	29.13	0.21
hsa-miR-30b-5p	29.17	0.26
hsa-miR-151a-3p	29.33	0.18
hsa-miR-328-3p	29.34	1.83
hsa-miR-133a-3p	29.35	0.22
hsa-miR-661	29.37	0.27
hsa-miR-625-3p	29.41	0.46
hsa-miR-539-5p	29.42	0.76
hsa-miR-34a-5p	29.45	0.64
hsa-miR-374a-5p	29.46	0.03
hsa-miR-382-5p	29.53	0.79
hsa-miR-425-5p	29.63	1.08
hsa-miR-125b-5p	29.65	0.02
hsa-miR-1290	29.65	0.48
hsa-miR-495-3p	29.67	0.02
hsa-miR-744-5p	29.71	0.25
hsa-let-7g-5p	29.71	0.00
hsa-miR-126-5p	29.76	0.01
hsa-miR-31-3p	29.82	0.53
hsa-miR-605-5p	29.96	2.13
hsa-miR-92a-3p	30.00	0.08

miRNA name	CT mean	SD
hsa-miR-30a-5p	30.08	0.50
hsa-miR-99b-5p	30.17	0.35
hsa-miR-1270	30.28	1.06
hsa-miR-1303	30.31	0.38
hsa-miR-212-3p	30.39	1.78
hsa-miR-494-3p	30.39	0.02
hsa-miR-99b-3p	30.42	0.48
hsa-miR-106b-5p	30.44	0.35
hsa-miR-1254	30.47	0.50
hsa-let-7d-5p	30.49	0.25
hsa-miR-339-3p	30.52	0.66
hsa-miR-668-3p	30.62	0.44
hsa-miR-7-1-3p	30.65	2.57
hsa-miR-433-3p	30.69	0.43
hsa-miR-143-3p	30.71	0.95
hsa-miR-181a-5p	30.74	0.36
hsa-miR-93-5p	30.78	1.05
hsa-miR-19a-3p	30.81	0.35
hsa-miR-638	30.82	0.61
hsa-miR-659-3p	30.83	0.51
hsa-miR-335-3p	30.84	2.04
hsa-miR-493-3p	30.85	0.25
hsa-miR-1271-5p	30.88	1.55
hsa-miR-27a-3p	30.91	0.89
hsa-miR-410-3p	30.93	0.41
hsa-miR-152-3p	30.93	1.01
hsa-miR-34a-3p	30.97	0.90
hsa-miR-425-3p	31.01	0.28
hsa-miR-636	31.03	0.06
hsa-miR-10a-5p	31.04	0.08
hsa-miR-26b-5p	31.17	1.11
hsa-miR-150-5p	31.17	0.82
hsa-miR-223-3p	31.18	0.55
hsa-miR-324-3p	31.22	0.20
hsa-miR-140-5p	31.26	1.27
hsa-miR-487b-3p	31.35	1.00
hsa-miR-136-3p	31.35	2.64
hsa-miR-655-3p	31.47	0.41
hsa-miR-1208	31.51	1.17
hsa-miR-483-5p	31.62	0.52
hsa-miR-379-5p	31.65	0.59

miRNA name	CT mean	SD
hsa-miR-195-5p	31.66	0.64
hsa-miR-943	31.67	0.23
hsa-miR-103a-3p	31.72	1.40
hsa-miR-590-5p	31.82	0.08
hsa-miR-335-5p	31.98	0.51
hsa-miR-132-3p	31.99	0.42
hsa-miR-708-5p	32.04	0.02
hsa-miR-144-3p	32.09	2.51
hsa-miR-15b-5p	32.12	1.04
hsa-miR-20b-5p	32.17	0.61
hsa-miR-323a-3p	32.20	0.10
hsa-miR-378a-3p	32.24	0.35
hsa-miR-93-3p	32.24	0.39
hsa-miR-1275	32.29	1.06
hsa-miR-28-5p	32.49	1.10
hsa-miR-629-3p	32.57	0.17
hsa-miR-485-3p	32.57	0.49
hsa-miR-218-5p	32.61	0.85
hsa-miR-1226-5p	32.67	2.87
hsa-miR-431-5p	32.76	1.19
hsa-miR-516b-3p	32.79	0.85
hsa-miR-365a-3p hsa-miR-365b-3p	32.84	0.21
hsa-miR-532-3p	32.97	0.61
hsa-miR-628-5p	33.01	1.37
hsa-miR-892b	33.02	2.16
hsa-miR-1291	33.02	0.29
hsa-miR-520b	33.05	0.71
hsa-miR-151a-5p	33.08	2.04
hsa-miR-29b-3p	33.11	0.34
hsa-miR-196b-5p	33.16	0.82
hsa-miR-130b-3p	33.22	4.69
hsa-miR-769-5p	33.24	5.66
hsa-miR-564	33.29	0.06
hsa-miR-424-3p	33.30	0.96
hsa-miR-455-5p	33.32	1.31
hsa-miR-889-3p	33.33	0.71
hsa-miR-200c-3p	33.44	5.56
hsa-miR-543	33.44	0.70
hsa-miR-650	33.44	6.21
hsa-miR-337-5p	33.44	0.19
hsa-miR-491-5p	33.45	6.13
hsa-miR-27a-5p	33.47	5.16
hsa-miR-25-3p	33.50	6.48
hsa-miR-338-5p	33.55	0.71
hsa-miR-214-5p	33.55	5.18
hsa-miR-320b	33.55	6.08
hsa-miR-140-3p	33.66	5.33
hsa-miR-340-5p	33.76	1.61
hsa-miR-26a-1-3p	33.82	1.24
hsa-miR-598-3p	33.90	1.28
hsa-miR-324-5p	33.91	5.97
hsa-miR-33a-5p	33.93	6.77
hsa-miR-589-3p	33.94	5.29
hsa-miR-520c-3p	33.98	0.62
hsa-miR-601	34.00	0.50
hsa-miR-29c-3p	34.16	0.26
hsa-miR-548c-3p	34.16	0.35
hsa-miR-18a-5p	34.17	0.26
hsa-miR-193a-5p	34.24	0.39
hsa-miR-301a-3p	34.33	4.99
hsa-miR-130a-3p	34.38	0.73
hsa-miR-939-5p	34.38	7.95
hsa-miR-486-5p	34.42	0.31
hsa-miR-125a-3p	34.48	0.24
hsa-miR-148b-3p	34.54	2.67

Table 3. *List of miRNAs carried by FIBRO EVs. Data are displayed as CT mean value ± SD (n=3). The 15 most expressed miRNAs, used in bioinformatics analysis, are highlighted in bold.*

Pathways enrichment analysis showed that these genes are involved in pathways related to EGFR, PDGFR, VEGF and TGFβ. Moreover, integrins and endothelins, mTOR and the Wnt pathway were also found significantly enriched (Figure 4).

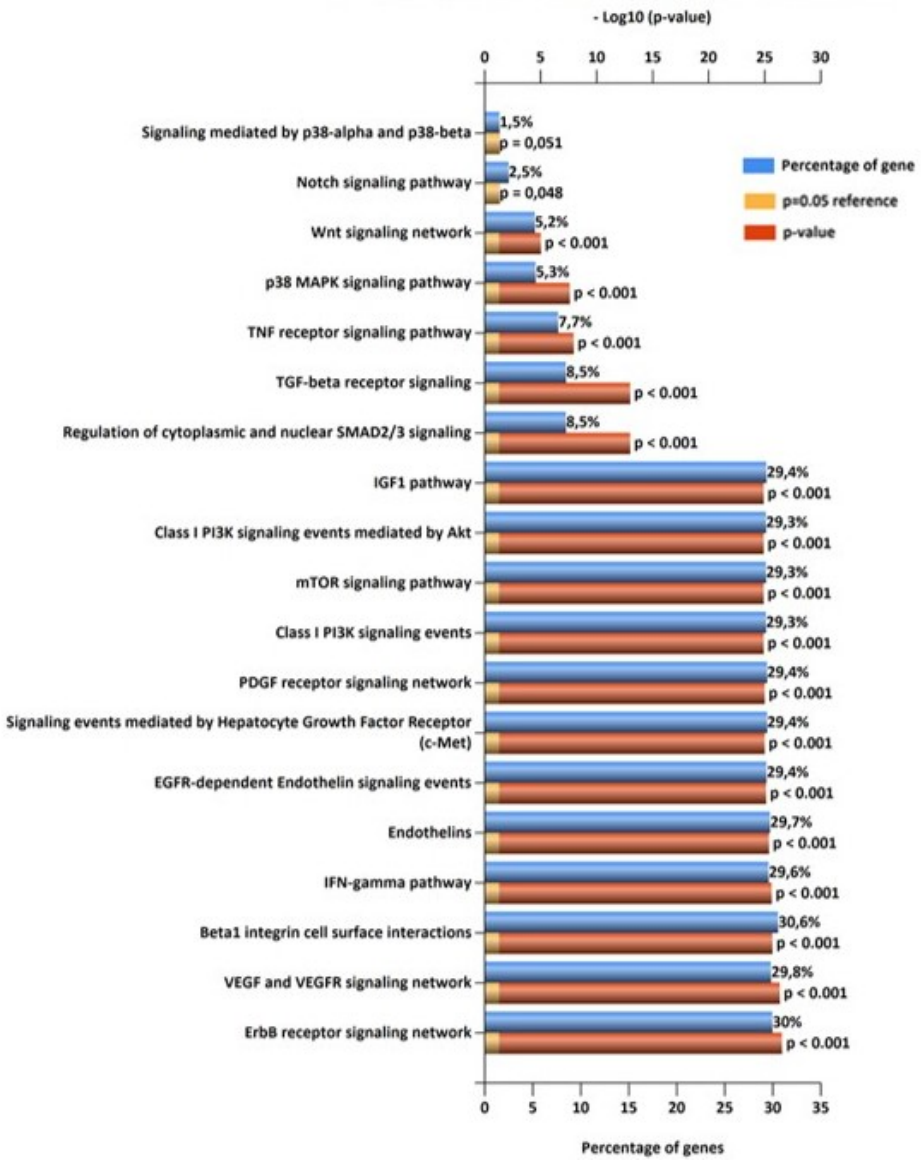

Figure 4. Pathway enrichment analysis of MSC EV specific miRNA targets. *p<0.05 Hypergeometric test with Bonferroni correction*

MSC EVs ameliorate renal function and decrease renal fibrosis (curative model)

We evaluated the potential anti-fibrotic effect exerted by MSC EVs in a DN model induced by STZ administration in NSG mice. This model recapitulates DN progression. Glycemia was measured (glycemia >250 mg/dl) every two weeks. Usually mice developed hyperglycemia (355± 85 mg/dl of glucose) ten days after STZ injection (T0). EV treatment started one months after (T28) the diabetes onset (Figure 5). Mice were treated for 4 consecutive weeks, once per week, at the concentration of $1x10^{10}$ MSC EVs each injection. FIBRO EVs were used as control (Figure 5).

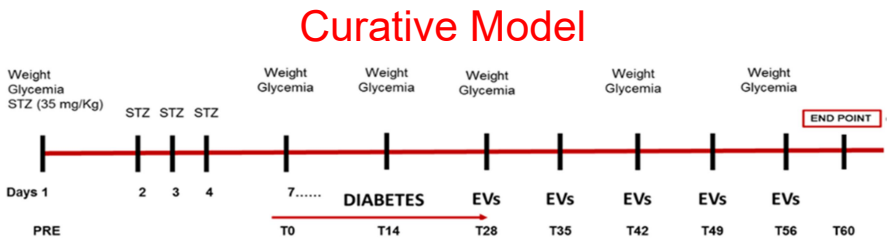

Figure 5. Scheme of DN model and timing of MSC EV administration. *MSC EVs were administered at day 28 (T28) after diabetes onset and then administered weekly (1x10^{10}/each injection) for four consecutive weeks. Mice were sacrificed at day 60 and histological and molecular analyses performed.*

On day 28, after diabetes onset, urinary albumin excretion, estimated as the albumin-to-creatinine ratio (ACR), was significantly higher in STZ-diabetic mice (CTL) than in healthy mice (Figure 6A). MSC EV treated mice showed a significant ACR reduction that was not observed in mice treated with FIBRO EVs (Figure 6A). Plasma creatinine and BUN levels were also found significantly higher in STZ-diabetic mice than in healthy ones, and their levels were partially restored after MSC EV administration (Figure 6B-C). Periodic Acid-Schiff (PAS) staining showed an increase in the Bowman's space in STZ-diabetic mice (Figure 6D) in accordance with DN-associated renal histopathological change. Moreover, trichrome staining revealed renal collagen deposition in the glomerular and interstitial renal spaces of STZ-diabetic mice (Figure 6E-F). All these histopathological features were restored by MSC EV treatment (Figure 6D-F), but not in response to FIBRO EVs.

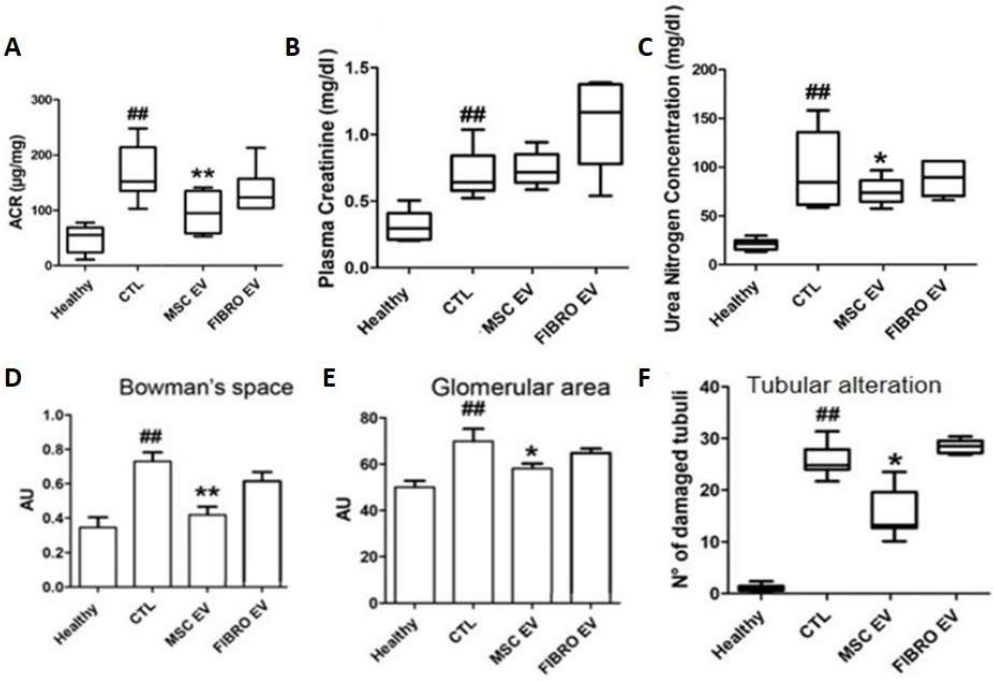

Figure 6. Biochemical and histological analyses of healthy, STZ-diabetic mice (CTL) mice compared to MSC EV or FIBRO EV treated mice at T60. *Biochemical analyses : A) albumin-to-creatinine ratio (ACR); B) Plasma Creatinine; C) Blood urea nitrogen (BUN). Data are expressed as mean ±SEM; ## $p<0.001$ versus healthy; * $p<0.05$ and ** $p<0.001$ versus CTL (n=8). Histological analyses: D) Bowman's space quantification;*

*E) quantification of Glomerular area; F) evaluation of tubular alteration. Data are expressed in AU (arbitrary units) as mean ±SEM; ## p<0.001 versus healthy; * p<0.05 and ** p<0.001 versus CTL (n=8). ANOVA with Dunnet's multi comparison test was performed. ANOVA with Dunnet's multi comparison test was performed. No significant differences were observed with CTL and FIBRO EV.*

MSC EVs decrease and partially revers renal fibrosis in ND mouse model

Kidneys of healthy, STZ-treated mice untreated or treated with MSC EVs or FIBRO EVs were evaluated by trichrome staining. On day 60 we observed a marked interstitial and glomerular fibrosis in CTL mice (diabetics) with respect to the healthy ones (Figure 7). Upon MSC EV administration, renal section showed a marked reduction of the interstitial and glomerular collagen deposition. These effects were not detected in mice that have been treated with FIBRO EVs (Figure 7).

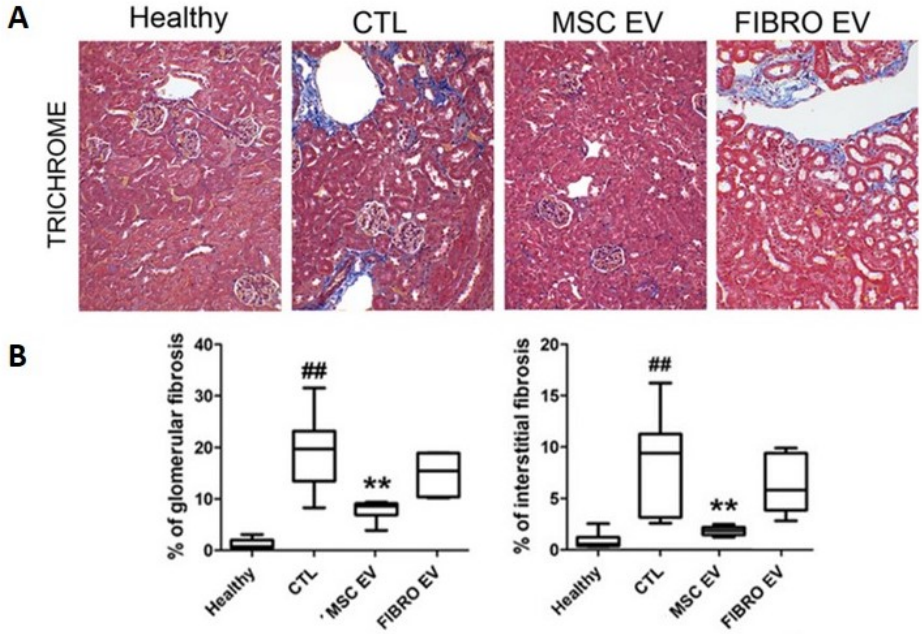

Figure 7. Renal fibrosis evaluation. *A) Representative images of Masson's trichrome sections of healthy, CTL and EV-treated mice (magnification: 200X). B) Quantification of glomerular and interstitial fibrosis. Data are expressed as percentage of fibrosis/glomerular area and percentage of fibrosis/total area. Data are expressed as mean ±SEM; ## p<0.001 versus healthy; ** p<0.001 versus CTL (n=8). ANOVA with Dunnet's multi comparison test was performed.*

We also evaluated the expression of typical fibrotic genes such as collagen I, TGF-β and α-SMA at the molecular level. The progressive accumulation of extracellular matrix components and the activation of fibrotic pathways were confirmed by the up-regulation of collagen I, TGF-β and α-SMA mRNAs in CTL with respect to healthy mice (Figure 8A). Their expression was significantly reduced after MSC EV treatment. No effects was observed in FIBRO EV injected mice, demonstrating the specific effect exerted by MSC EVs.

The expression of fibrotic genes worsens over time as a consequence of the hyperglycemic condition (Fig. 8B). However, their expression levels in MSC EV-treated mice on day 60 was significantly reduced (Figure 8C). TGF-β mRNA expression did not increase in MSC EV treated animals compared to untreated ones (Figure 8C), suggesting a reversion of the fibrotic process.

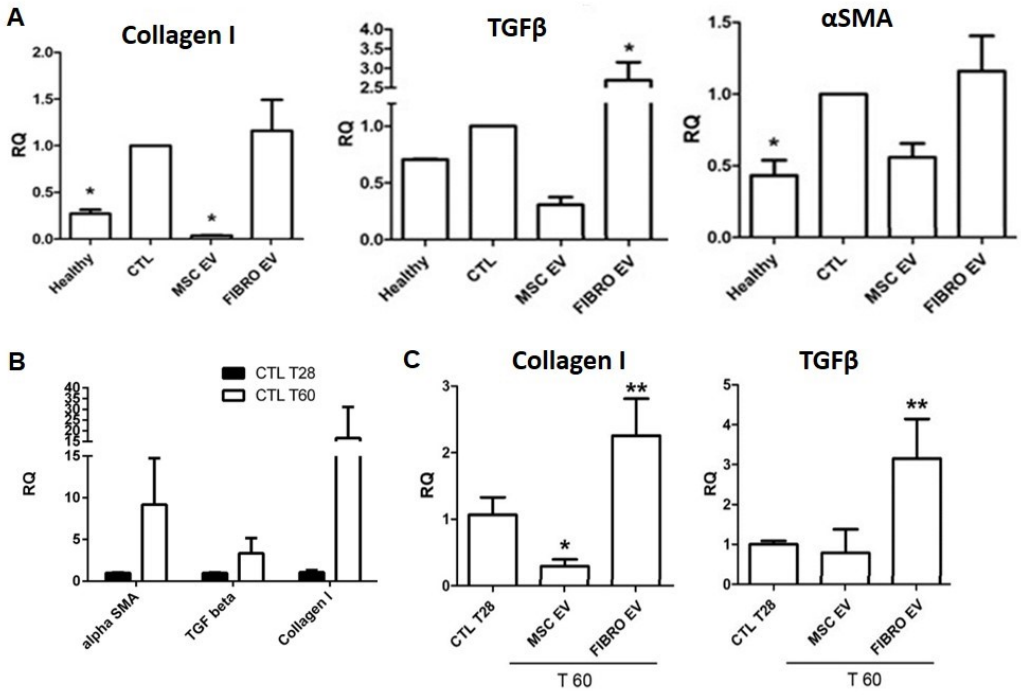

Figure 8. Fibrotic genes expression DN mouse model. *Gene expression levels of collagen I, TGF-β and α-SMA in STZ-diabetic mice analyzed 60 days after the onset of diabetes treated or not with MSC EVs. Data are normalized to GAPDH and to 1 for CTL, and are expressed as Relative Quantification ±SD (n=4); * p<0.05 and ** p<0.001 versus CTL. ANOVA with Dunnet's multi comparison test was performed.*

To better elucidate the protective effect of MSC EVs at the molecular levels, the regulation of genes associated to fibrosis was investigated. PCR array was performed on renal tissue of healthy, CTL and MSC EV treated mice, analysing 84 genes involved in fibrosis (Figure 9). Clustering analyses, represented in the heatmap (Figure 9A), revealed a clear pattern of genes modulated in diabetic mice with respect to healthy controls (Figure 9A). The expression of a cluster of genes, which includes metalloproteinase 3 (MMP3), Serpina1, interferon γ, Fas Ligand, collagen I and chemokine (C-C motif) ligand 3 (CCL3), also known as macrophage inflammatory protein 1α (MIP-1α), was completely restored by MSC EV treatments (Figure 9B). In particular, a comparison between healthy and DN mice revealed that fifteen of the 84 genes analyzed were downregulated, while nineteen were upregulated in DN mice. Twelve genes upregulated in CTL mice were downregulated by MSC EV treatment, while five upregulated in DN mice were reverted in MSC EV injected mice. Interestingly, the expression

of these genes in MSC EV treated mice was similar to that of the healthy group (Figure 9A-B).

A

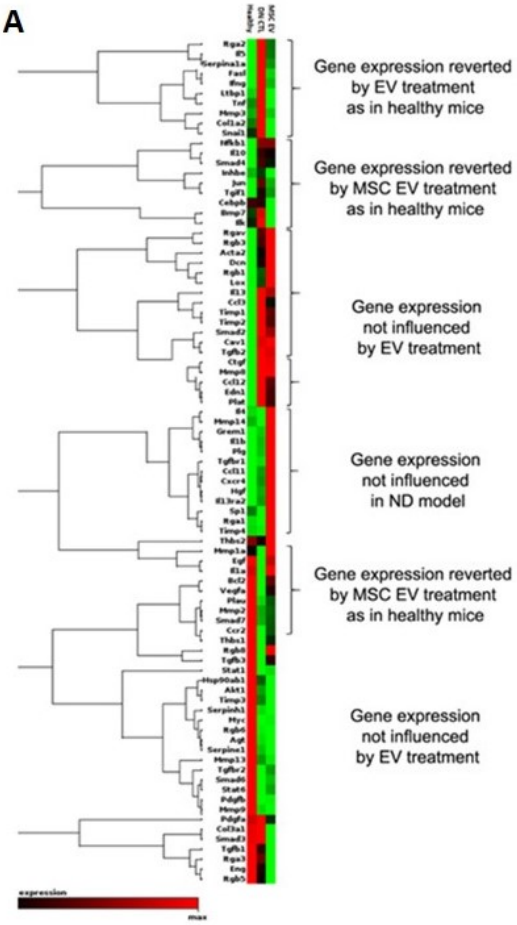

B

	Fold Change	
Gene name	**CTL**	**MSC EV**
Fasl	4.806	0.270
Serpina1a	6.723	0.316
Mmp3	2.505	0.357
Itga2	4.507	0.433
Ifng	2.796	0.438
Bmp7	1.496	0.450
Il5	3.149	0.495
Col1a2	1.591	0.501
Ccl3	5.653	0.557
Inhbe	1.407	0.562
Tnf	1.515	0.562
Snai1	1.356	0.562
Il1a	0.257	4.116
Mmp1a	0.546	2.723
Ccr2	0.199	2.342
Bcl2	0.436	1.890
Tgfb3	0.416	1.830

Figure 9. Fibrosis associated gene expression analysis. A) Heatmap displaying hierarchical clustering of the entire dataset of expressed genes in the different experimental groups: healthy, STZ-diabetic mice (CTL), and MSC EV treated mice. Clustering analysis showed that some groups of genes altered in DN were restored to healthy levels via treatment with MSC EVs (n=3 for each experimental condition). B) List of genes altered in DN and reverted by MSC EV administration. Data are represented as fold change of STZ-diabetic mice with respect to healthy (CTL column) and CTL mice and are compared with MSC EV treated mice (MSC EV column).

MSC EV treatment ameliorate fibrosis soon after diabetes onset

It was demonstrated a correlation between autophagy and fibrosis [73]. Since the above described model is not suitable to investigate autophagy due to the extent of fibrosis in DN control mice, the effect of MSC EV treatment on autophagy was investigated at an earlier stage of disease. To this end, diabetes was induced in NSG mice by STZ injection while treatment started just after diabetes onset (up to 250 mg/ml-T0). Glycaemia was monitored every 2 weeks. Mice were treated by intravenously injecting $1x10^{10}$ MSC EVs/ each injection for 4 consecutive weeks (Figure 10).

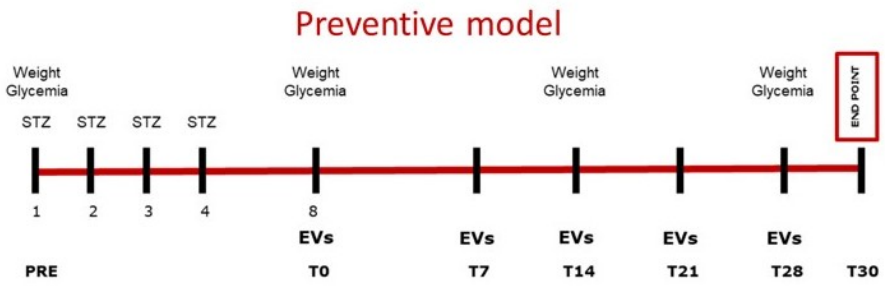

Figure 10. Scheme of early DN model and timing of MSC EV administration. *MSC EVs were administered after diabetes onset (T0) and then administered weekly (1x10^{10}/each injection) for four consecutive weeks. Mice were sacrificed at day 30 and histological and molecular analyses were performed.*

After 30 days from diabetes onset, all renal biochemical parameter ACR, creatinine and BUN were increased in STZ-mice, confirming the renal damage (Figure 6A-C). The protective effect of MSC EVs was also confirmed at this DN stage. In fact, ACR, BUN and creatinine levels are decreased compared to diabetic mice. Histological analysis of CTL and DN kidney sections showed an increase of Bowman's space and the establishment of renal fibrosis. As shown in Figure 11 MSC EV treatment was able to restore histological features.

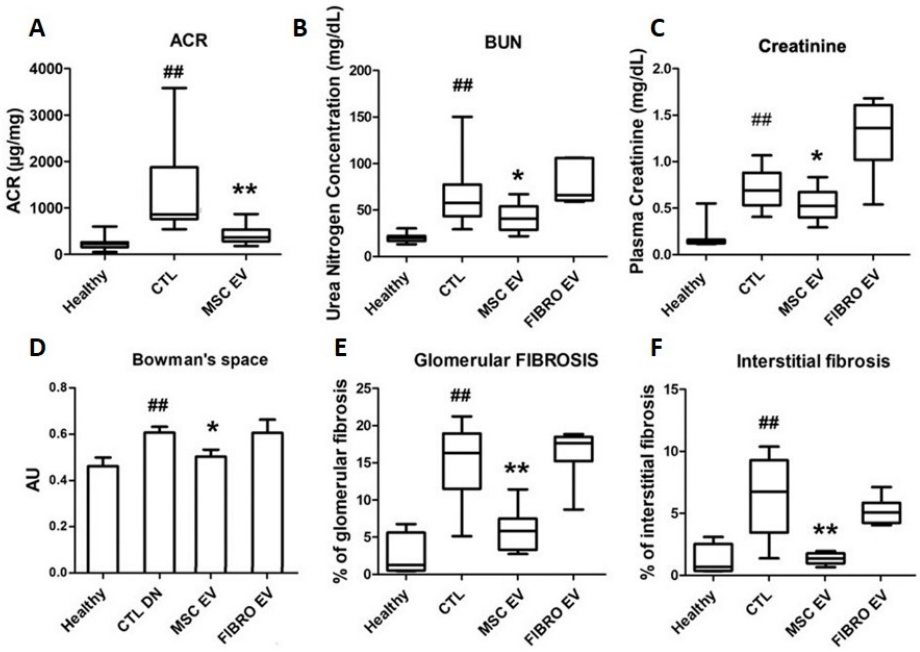

Figure 11. Biochemical and histological analyses of healthy, STZ-diabetic mice (CTL) mice compared to MSC EV or FIBRO EV treated mice at T28. *Biochemical analyses: A) albumin-to-creatinine ratio (ACR); B) Blood urea nitrogen (BUN); C) Plasma Creatinine. Data are expressed as mean ±SEM; # p<0.05 and ## p<0.01 in respect to healthy mice (n=8). Histological analyses: D) Bowman's space quantification. Data are expressed in AU (arbitrary units) as mean ±SEM; # p<0.05 versus healthy; * p<0.05 versus CTL (n=8); E) Quantification of glomerular and F) interstitial fibrosis. Data are expressed as percentage of fibrosis/glomerular area and percentage of fibrosis/total area. Data are expressed as mean ±SEM; ## p<0.001 versus healthy; ** p<0.001 versus CTL (n=8). ANOVA with Dunnet's multi comparison test was performed. No significant differences were observed with CTL and FIBRO EV.*

The possibility that MSC EVs could protect renal tubules from programmed cell death was therefore investigated. Kidney sections were stained by TUNEL and positive cells were counted. As reported in Figure 12, MSC EV treatment reduced the number of apoptotic tubular cells.

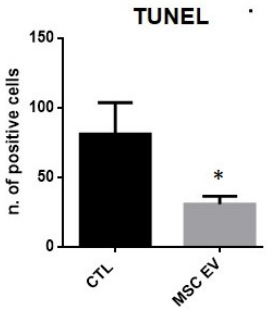

Figure 12. TUNEL assay in DN mice treated or not with EVs. *MSC EV treatment reduce the number of positive tubular cells. Data are expressed as mean ±SEM of 5 mice per group. P<0.05 CTL vs MSC EV; Student T test was performed.*

MSC EVs slightly modulate autophagy in DN renal tissue

Preliminary studies were performed to evaluate autophagy in renal sections. Immunofluorescence staining for the typical autophagic marker LC3B showed an increased formation of small LC3 positive aggregates in tubular cells of diabetic CTL mice. On the contrary a diffuse staining in the whole cytoplasm was detected in healthy control. These data suggest an increased activation of the autophagic process (Figure 13), however, since the total LC3B staining did not discriminate between the LC3BI and the active LC3BII form, the possibility that accumulation of LC3B positive vesicles may be due to the blockade of autophagy can not be excluded. Nevertheless, MSC EV administration induce the formation of bigger LC3 puncta in some tubules, and similar to healthy control a diffuse staining was detected in most tubular cells (Figure 13).

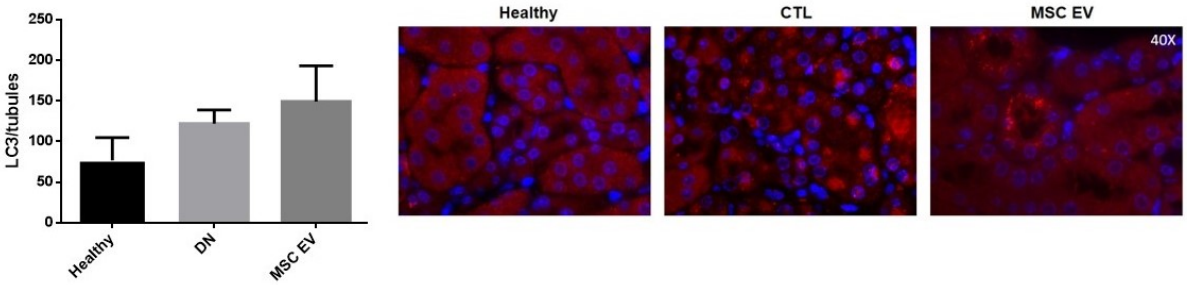

Figure 13. LC3B staining of DN mice kidney sections*. Representative micrographs of LC3B staining in healthy, CTL and MSC EV treated mice; 400X magnification. Quantification of puncta in tubules of healthy, CTL DN and MSC EV treated mice. (n=5 mice per group; 7 field per mouse).*

To better investigate the autophagic flux, western blot analysis was performed on kidney tissues. We noticed a reduction of LC3BII/I ratio in CTL mice that slightly increased after MSC EV treatment. We also evaluate the expression of p62, a protein involved in the maturation of the autophagosome. The expression of p62 decreased in DN mice with respect to healthy and the same pattern of expression was observed in MSC EV treated mice. A reduction of the autophagy flux due to downregulation of p62 or the enhancement of the autophagic flux resulting in p62 degradation can be postulated to explain these results (Figure 14).

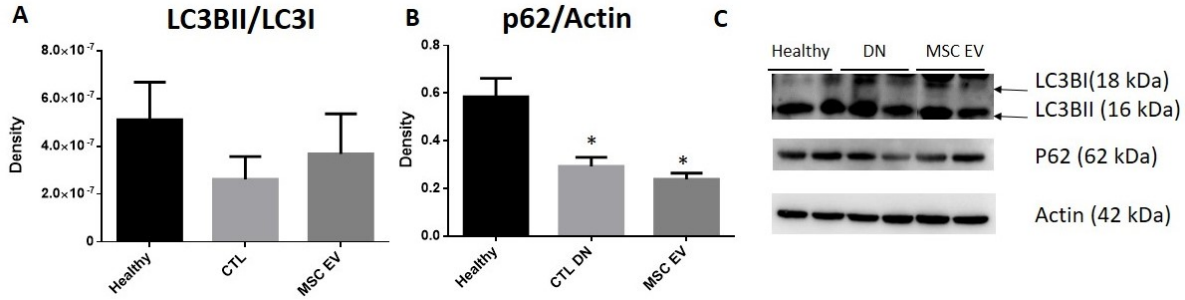

Figure 14. Western blot analysis on DN kidney tissue. *A) and B) LC3BII and p62 densitometric quantification (n=5 mice per group); βActin was used as endogenous control for protein loading. *p<0.05 versus healthy ANOVA with Dunnet's multi comparison test was performed; C) Representative western blot of LC3BI (upper band) and LC3BII (lower band), p62 and βactin, used ad endogenous control.*

To better investigate the effect of MSC EVs treatment the expression of genes related to autophagy were also evaluated. We performed PCR array on autophagy related genes and we observed that two genes were downregulated in CTL mice at month 1 with respect to healthy animals, whereas nine were upregulated. Of note, the anti-apoptotic Bcl2 was reduced while the pro-apototic Bax was increased in ND mice. In mice treated with MSC EVs decreased expression of several genes encoding for proteins involved at different stages of autophagy, such as activation (Beclin, ULK1, AMBRA and AKT), formation of autophagosome (ATG12, ATG7, ATG9, WIPI) and expansion of autophagosome (SQSTM1, GABARAPL1) were detected (Figure 15). Of interest, several genes were reduced in MSC EV treated mice recapitulating the healthy ones (Figure 15D).

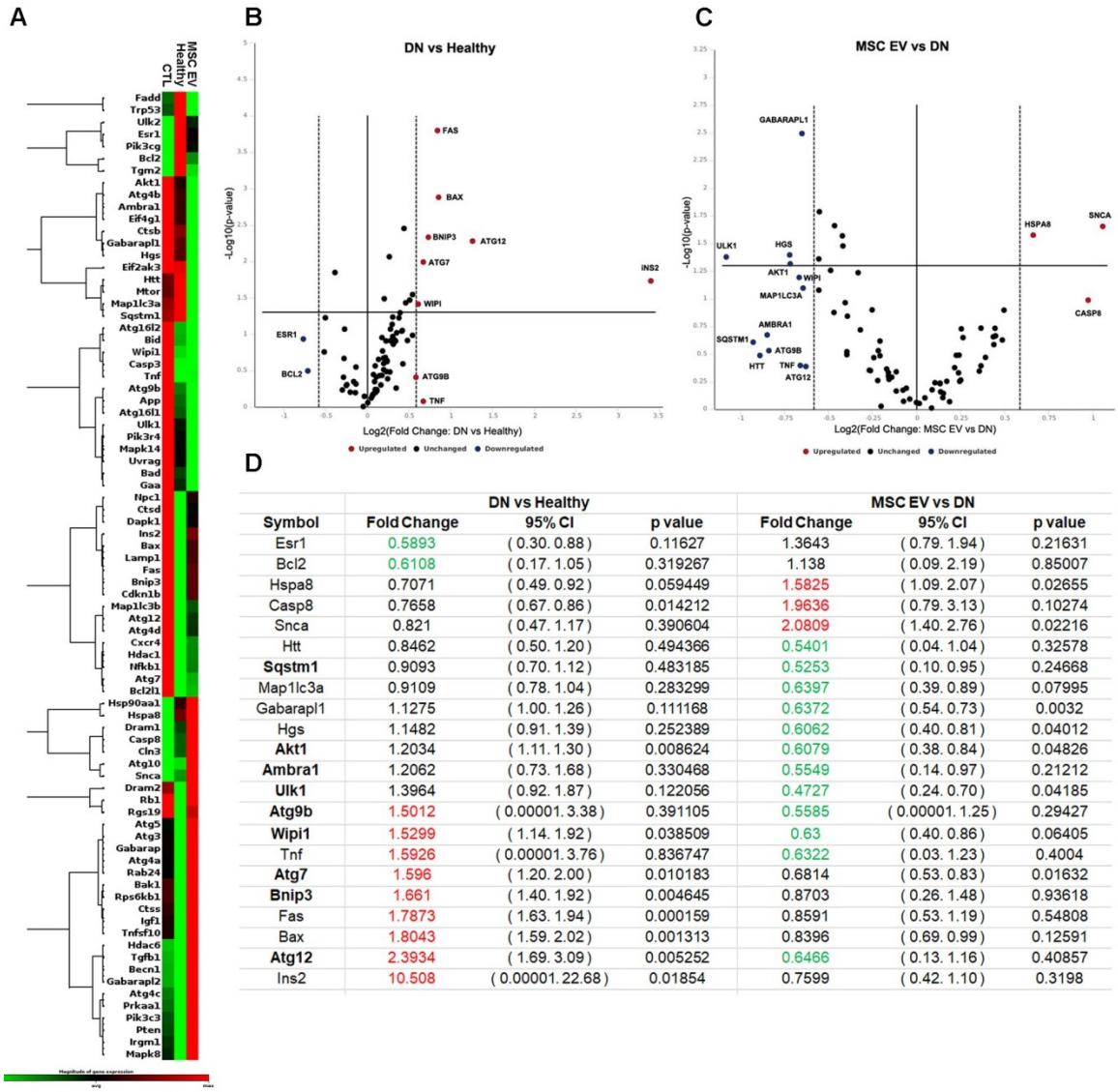

D

	DN vs Healthy			MSC EV vs DN		
Symbol	**Fold Change**	**95% CI**	**p value**	**Fold Change**	**95% CI**	**p value**
Esr1	0.5893	(0.30. 0.88)	0.11627	1.3643	(0.79. 1.94)	0.21631
Bcl2	0.6108	(0.17. 1.05)	0.319267	1.138	(0.09. 2.19)	0.85007
Hspa8	0.7071	(0.49. 0.92)	0.059449	1.5825	(1.09. 2.07)	0.02655
Casp8	0.7658	(0.67. 0.86)	0.014212	1.9636	(0.79. 3.13)	0.10274
Snca	0.821	(0.47. 1.17)	0.390604	2.0809	(1.40. 2.76)	0.02216
Htt	0.8462	(0.50. 1.20)	0.494366	0.5401	(0.04. 1.04)	0.32578
Sqstm1	0.9093	(0.70. 1.12)	0.483185	0.5253	(0.10. 0.95)	0.24668
Map1lc3a	0.9109	(0.78. 1.04)	0.283299	0.6397	(0.39. 0.89)	0.07995
Gabarapl1	1.1275	(1.00. 1.26)	0.111168	0.6372	(0.54. 0.73)	0.0032
Hgs	1.1482	(0.91. 1.39)	0.252389	0.6062	(0.40. 0.81)	0.04012
Akt1	1.2034	(1.11. 1.30)	0.008624	0.6079	(0.38. 0.84)	0.04826
Ambra1	1.2062	(0.73. 1.68)	0.330468	0.5549	(0.14. 0.97)	0.21212
Ulk1	1.3964	(0.92. 1.87)	0.122056	0.4727	(0.24. 0.70)	0.04185
Atg9b	1.5012	(0.00001. 3.38)	0.391105	0.5585	(0.00001. 1.25)	0.29427
Wipi1	1.5299	(1.14. 1.92)	0.038509	0.63	(0.40. 0.86)	0.06405
Tnf	1.5926	(0.00001. 3.76)	0.836747	0.6322	(0.03. 1.23)	0.4004
Atg7	1.596	(1.20. 2.00)	0.010183	0.6814	(0.53. 0.83)	0.01632
Bnip3	1.661	(1.40. 1.92)	0.004645	0.8703	(0.26. 1.48)	0.93618
Fas	1.7873	(1.63. 1.94)	0.000159	0.8591	(0.53. 1.19)	0.54808
Bax	1.8043	(1.59. 2.02)	0.001313	0.8396	(0.69. 0.99)	0.12591
Atg12	2.3934	(1.69. 3.09)	0.005252	0.6466	(0.13. 1.16)	0.40857
Ins2	10.508	(0.00001. 22.68)	0.01854	0.7599	(0.42. 1.10)	0.3198

Figure 15. Autophagy related genes expression analysis in DN mice after 1 month of diabetes*. A) Heatmap clustering analysis. B) Volcano Plot showing Relative Quantification (RQ) of CTL DN mice gene expression in respect to the healthy (n=3). C) Volcano Plot showing Relative Quantification (RQ) of MSC EV treated mice gene expression in respect to CTL (n=3). Horizontal lines represents p value<0.05. D) Table showing genes modulated in CTL vs Healthy (first column) and MSC EV vs CTL. RQ CI 95% and p<0.05 (t-test).*

Validation of modulated genes in renal tissue of healthy, CTL and MSC EV treated mice was further performed. We confirmed that MSC EV treatment was associated with a general downregulation of key genes involved at different stages of autophagy (Figure 16). Some of them (ULK1, WIPI1, BNIP3) were significantly downregulated with respect to diabetic CTL mice.

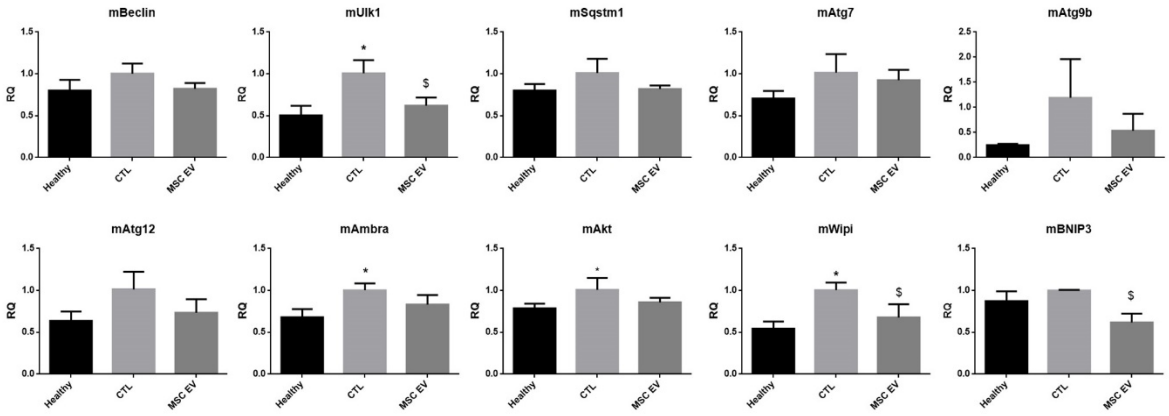

Figure 16. Real time validation of autophagy related genes differentially expressed in DN mice at 1 month after diabetes onset. *Data are expressed as Relative Quantification (RQ) ±SD *p<0.05 CTL vs Healthy; $ p<0.05 CTL vs MSC EV ANOVA with Dunnet's multi comparison test was performed*

MSC EV cargo could modulate the autophagy cascade

Molecules potentially involved in the control of the autophagy cascade and regulated by MSC EVs were also evaluated in detail. Bioinformatic was interrogated to predict miRNAs targets using miRwalk. We noticed that among MSC EV miRNAs, 160 are involved in the regulation of autophagy/mitophagy related genes, suggesting that the delivery of these miRNAs by MSC EVs can be involved in these processes (Figure 17).

AUTOPHAGY

gene name	#miRNA
ATG10	21
ATG101	4
ATG12	28
ATG13	30
ATG16L1	35
ATG2A	10
ATG2B	31
ATG3	3
ATG4A	14
ATG4B	22
ATG4C	14
ATG4D	7
ATG5	21
ATG7	25
ATG9A	7
ATG9B	10
BECN1	8
GABARAP	12
GABARAPL1	30
GABARAPL2	4
IGBP1	8
MLST8	9
mTOR	3
PIK3C3	2
PPP2CA	15
PPP2CB	4
RPTOR	5
ULK2	24
ULK1	11
WIPI1	7
WIPI2	29

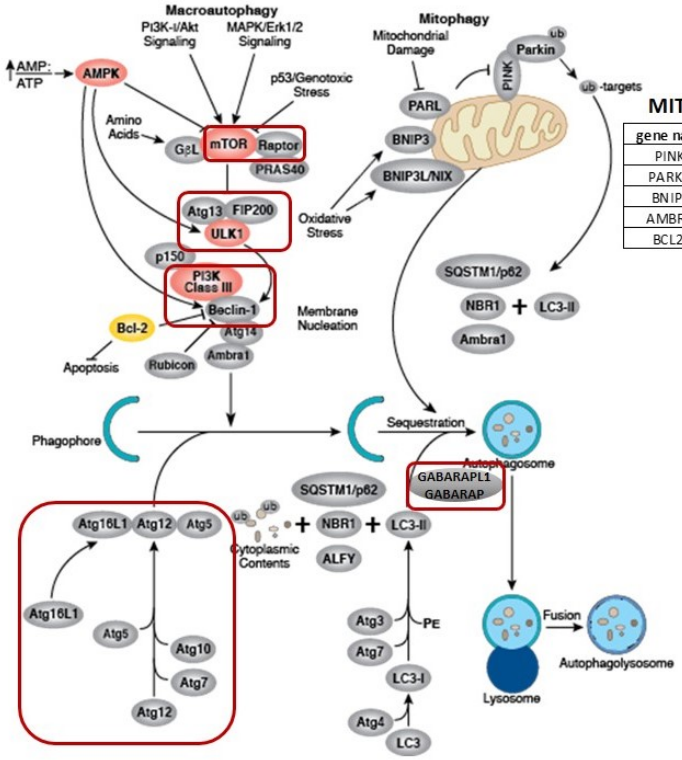

MITOPHAGY

gene name	#miRNA
PINK1	5
PARKIN	41
BNIPL3	35
AMBRA1	20
BCL2L1	46

Figure 17. *Schematic representation of genes involved in the autophagy cascade (mTOR, ULK1/2, GABARAP and GABARAPL1, ATGs) and targeted by MSC EV-miRNAs.*

We have also evaluated whether MSC EV protein content could also be involved in these processes. As shown in Table 3, among proteins contained in MSC EVs, PPARG, CREBBP were found. These two transcription factors are involved the DN pathogenesis as well as in the regulation of PI3K, WNT, JAK/STAT and AMPK (Table 5 and 6).

Table 5. CREBBP regulated pathways

# KEGG term	# of overlapped genes	P value	FDR
Glucagon signaling pathway	5	2.74E+08	3.71E+07
PI3K-Akt signaling pathway	7	3.91E+08	5.64E+07
Circadian rhythm	3	5.96E+09	1.40E+09
HIF-1 signaling pathway	4	6.66E+09	1.60E+09
FoxO signaling pathway	4	1.57E-04	4.45E+09
Jak-STAT signaling pathway	4	2.69E-04	8.41E+09
Central carbon metabolism in cancer	3	3.96E-04	1.36E-04
Insulin resistance	3	1.21E-03	5.62E-04
TNF signaling pathway	3	1.24E-03	5.77E-04
Cell cycle	3	1.62E-03	8.15E-04
Oxytocin signaling pathway	3	2.84E-03	1.63E-03
Pyruvate metabolism	2	2.88E-03	1.66E-03
cAMP signaling pathway	3	4.80E-03	3.13E-03
Arachidonic acid metabolism	2	5.71E-03	3.88E-03
Glycolysis / Gluconeogenesis	2	6.45E-03	4.51E-03
p53 signaling pathway	2	6.62E-03	4.64E-03
PPAR signaling pathway	2	6.79E-03	4.77E-03
Adipocytokine signaling pathway	2	6.94E-03	4.91E-03
Adherens junction	2	7.43E-03	5.32E-03
Cytokine-cytokine receptor interaction	3	9.27E-03	6.92E-03
ErbB signaling pathway	2	9.86E-03	7.44E-03
Hematopoietic cell lineage	2	9.86E-03	7.44E-03
Estrogen signaling pathway	2	1.22E-02	9.52E-03
T cell receptor signaling pathway	2	1.32E-02	1.05E-02
Serotonergic synapse	2	1.49E-02	1.20E-02
Thyroid hormone signaling pathway	2	1.62E-02	1.33E-02
AMPK signaling pathway	2	1.76E-02	1.46E-02
Dopaminergic synapse	2	1.88E-02	1.57E-02
Wnt signaling pathway	2	2.18E-02	1.85E-02
MAPK signaling pathway	2	5.85E-02	5.45E-02

Table 5. CREBBP regulated pathways analysed with TRUUST database. P<0.05 and FDR<0.05

Table 6. PPARG regulated pathways			
# KEGG term	**# of overlapped genes**	**P value**	**FDR**
PPAR signaling pathway	9	4.92E+03	1.91E+02
PI3K-Akt signaling pathway	13	2.35E+05	1.31E+04
p53 signaling pathway	6	1.04E+08	1.24E+07
Thyroid hormone signaling pathway	7	1.27E+08	1.57E+07
FoxO signaling pathway	7	2.74E+07	3.72E+07
Apoptosis	6	3.29E+08	4.64E+07
Jak-STAT signaling pathway	7	7.05E+08	1.12E+08
TNF signaling pathway	6	1.19E+09	2.09E+08
AMPK signaling pathway	6	2.12E+09	4.17E+08
NF-kappa B signaling pathway	5	6.39E+09	1.52E+09
HIF-1 signaling pathway	5	0.000106	2.75E+09
Insulin resistance	5	0.000132	3.60E+09
Regulation of lipolysis in adipocytes	4	0.000149	4.18E+09
Cell cycle	5	0.000221	6.64E+09
Focal adhesion	6	0.000243	7.46E+08
Adipocytokine signaling pathway	4	0.000308	9.93E+09
Ras signaling pathway	6	0.000366	0.000124
ErbB signaling pathway	4	0.000597	0.000228
cAMP signaling pathway	5	0.001262	0.00059
MAPK signaling pathway	5	0.003044	0.001772
Non-alcoholic fatty liver disease (NAFLD)	4	0.003052	0.001778
Hippo signaling pathway	4	0.003228	0.00191
Leukocyte transendothelial migration	3	0.010169	0.007729
Sphingolipid signaling pathway	3	0.010576	0.008089
Tryptophan metabolism	2	0.011066	0.00854
Fat digestion and absorption	2	0.011524	0.008948
Fatty acid degradation	2	0.012931	0.010221
Insulin signaling pathway	3	0.014869	0.012013
Notch signaling pathway	2	0.014887	0.012036
Type II diabetes mellitus	2	0.014887	0.012036
Fatty acid metabolism	2	0.014887	0.012036
Wnt signaling pathway	3	0.01538	0.012479
Cytokine-cytokine receptor interaction	4	0.015646	0.012726
Adrenergic signaling in cardiomyocytes	3	0.01723	0.014192
VEGF signaling pathway	2	0.022074	0.018816
Rap1 signaling pathway	3	0.039143	0.035401
Hematopoietic cell lineage	2	0.039787	0.03601
Regulation of actin cytoskeleton	3	0.040441	0.036671
Pancreatic secretion	2	0.046869	0.042959
Estrogen signaling pathway	2	0.049329	0.045379

Table 6. PPARG regulated pathways analysed with TRUUST database. P<0.05 and FDR<0.05

DISCUSSION

Many studies have suggested that stem cells and in particular mesenchymal stem cells from different sources (umbical cord blood, adipose tissue, bone marrow, amniotic fluid) may represent a useful DN treatment option [110-113]. However, cell-based therapy is associated with several side effects including host immune system stimulation and tumorigenicity. In this scenario stem cell-derived EVs have emerged as an alternative therapeutic approach for tissue regeneration with a superior safety profile [90, 114]. As a matter of fact, EVs intravenously injected preferentially home to the site of damage and exert similar effects of their cell of origin [115-117].

The healing properties of stem cell-derived EVs have been described in several pre-clinical models of disease [118, 119] including AKI and CKD [90].

For example, MSC EVs isolated from bone marrow and from cord blood were found effective in cisplatin lethal and sub-lethal models of AKI as they increased survival [120] and protected kidneys from oxidative stress-induced apoptosis [121].

On the contrary, the effect of EVs on CKD models has been poorly addressed. In particular, to prove EV efficacy in CKD, their preventive therapeutic effects should be separated from those exerted on late fibrotic events. The preventive approach mainly recapitulates the healing properties of EV that have been observed in AKI [90]. In this regard, Jiang *et al.* have reported that urine-purified MSC EVs prevent the development of DN [95]. A similar preventive effect has been reported after a single EV administration by Nagaishi *et al.* [96].

The present study demonstrates that MSC EVs exert beneficial effect on DN progression in NSG mice induced by STZ administration. The recovery of the kidney function associated with MSC EV treatment is sustained by the restoration of the urinary volume and water uptake, as well as by the renal physiological parameters including ACR, BUN and plasma creatinine. Fibrosis progression is also weakened by MSC EV administration, as demonstrated by the kidney morphology showing a reduction of tubular damage and glomerular and tubulo-interstitial fibrosis. MSC EV-mediated antifibrotic and protective effects was already evident after treatment of mice 1 month later the onset of diabetes. Moreover, MSC EV treatment not only prevented, but also reverted kidney fibrosis, as demonstrated by the morphological and molecular analyses of the kidney. Evidence for the specific effects of MSC-derived EV is further supported by the observation that FIBRO EVs were ineffective.

ECM protein deposition in the interstitial and glomerular space is one of the most relevant DN features [13]. The progressive decline of renal function strongly correlates with the development of glomerular and interstitial fibrosis [49]. Morphometric analyses coupled with

collagen I and α-SMA mRNA expression in the renal tissues of EV-treated animals indicated that MSC EVs inhibit the fibrotic process and CKD progression. Moreover, the observation that fibrosis and collagen I expression in renal tissues were significantly reduced in MSC EVs treated mice, and almost recapitulated the healthy tissues, suggests that a partial tissue rescue occurred. Consistently TGF-β expression was not increased in DN treated mice. Moreover, genes involved in the development of DN, such as Serpina1, FAS ligand, CCL3, TIMP1, MMP3, collagen I and SNAI1, were found downregulated in the renal tissue of MSC EVs treated animals. More importantly, their expression levels were comparable to those of healthy animals. EMT plays a fundamental role in DN progression and contributes to the early fibrotic events. Snail (gene name: SNAI1) is considered an early and crucial regulator of EMT [122]. Snail modulates tubulointerstitial fibrosis by repressing the expression of E-cadherin and by inducing the expression of α-SMA, fibronectin and collagen I in myofibroblasts [123]. We found that MSC EVs down-regulated Snail and collagen 1 expression in renal tissues. Metalloproteinases (MMPs) and tissue inhibitor of metalloproteinases (TIMP), proteins involved in ECM deposition/remodeling, are also dysregulated during DN progression [124, 125]. The increased expression of MMP3 (also called stromelysin) and TIMP1 have been reported in a rat model of STZ-induced DN [126]. Similar changes were observed in our experimental mouse model and MSC EV treatment completely restored their expression. Moreover, Serpina1 (α-1-antitrypsinin), which has been proposed as a urinary and serum DN biomarker [127, 128], was found the most upregulated molecule in our model of DN and, once again, its expression was completely reverted by MSC EV administration. The FAS ligand, which is known to regulate the survival of interstitial fibroblasts in the kidneys [129], has also been found to be upregulated in a chronic cyclosporine nephrotoxicity model [130]. In our experimental model, the expression of the FAS ligand was comparable to that of healthy controls after MSC EV treatment. Finally, CCL3/MIP-1α, which is one of the most relevant chemokines involved in the recruitment of monocyte/macrophages and T lymphocytes during renal inflammation in humans and proposed as a new therapeutic target for AKI and CKD, was found to be significantly downregulated in the kidneys of DN animals that were treated with MSC EVs [131].

Several studies have suggested a link between the development of fibrosis and autophagy [71, 73]. Activation of autophagy can be considered as the cell defence against several stress stimuli and its dysregulation has been linked to disorders characterized by fibrosis in various tissues, including idiopathic pulmonary fibrosis, liver fibrosis, cardiac fibrosis, and renal fibrosis [132, 133]. It has been demonstrated that in UUO, a well-established model of progressive renal interstitial fibrosis, autophagy is activated via the Akt-mTOR signalling

pathway. Moreover, its induction preceded both tubular apoptosis and interstitial fibrosis and peaked 3 days after the induction of UUO in the obstructed kidney. Inhibition of autophagy using 3-methyladenine (3-MA- an inhibitor of autophagosome formation via the blockade of type III PI-3K) enhanced tubular cell apoptosis and interstitial fibrosis [134]. These data indicate that autophagy exerts cytoprotective effect alleviating tubular damage and kidney fibrosis. Autophagy dysregulation was also described in DN [134]. Several studies have investigated the role of stem cell derived EVs in DN focusing on the autophagy cascade. Bone marrow rat MSC derived exosomes were found to improve renal function and restore renal morphology in a STZ induced DN rat model. Moreover, mouse-derived MSC EVs were reported to enhance autophagy by significantly increasing LC3 and Beclin-1, and decreasing the expression of both mTOR and fibrotic markers in renal tissues of db/db mice. This resulted in the mitigation of DN progression [88]. ADSC EVs exert similar effects by inducting autophagy and inhibiting the activation of mTOR signalling through miR-486 [102]. Furthermore, ADSC EV reduced urinary protein level and ameliorate renal biochemical parameter (creatinine and Blood urea nitrogen) and podocyte apoptosis *in vivo* [102].

In the present study we showed that autophagy is already dysregulated in diabetic mice at one month after diabetes onset, as confirmed by the expression of LC3 and p62. We noticed that LC3II/I and p62 were reduced in DN control mice and was partly restored by MSC EV treatment. Immunofluorescence study showed that altered autophagy occurs mainly in tubular cells. We observed an increase of LC3 positive puncta in DN control mice that became more evident in some tubules after MSC EV administration. Moreover, we observed a general downregulation of genes involved in different steps of the autophagy cascade, suggesting a regulation at different levels. ULK1 which is involved in autophagy initiation and regulated by AMPK, was reported as dysregulated in DN [68]. We showed that ULK1 and several ATGs are regulated by MSC EV treatment. Further studies will be performed to investigate the involvement of AMPK and ULK in STZ induced DN model and in particular on tubular cells.

To identify molecules shuttled by MSC EVs and accountable for these effects is challenging. In the last decades, several studies were performed to characterize nucleic acid (mRNA, miRNA, lncRNA), protein, bioactive lipid MSC EV cargo [84, 85]. Previously, differential ultracentrifugation was applied to identify the most active fraction involved in AKI protection. Data provided by this analysis indicate that the most biological activity was present in the 100K fraction, enriched in exosomes, rather than in the 10K fraction, enriched in shedding vesicles [135]. However, the best protective activity was obtained using the total fraction, containing both exosomes and microvesicles, and potentially acting synergistically

[135, 136]. In this study we characterized miRNA (by PCR array screening) and protein (by antibody based array screening) content of total MSC EV population. Taking into consideration the most abundant miRNAs differentially expressed by MSC EVs and FIBRO EVs, a specific miRNA signature was identified predicting MSC EV mechanism of action. Consistent with their therapeutic effects, bioinformatics analyses indicated that most miRNAs carried by MSC EVs target profibrotic pathways, such as TGF-β, WNT, EGFR and PDGFR [3, 7]. Among the most expressed miRNAs in MSC EVs, miRNA-29a, let-7 family, miRNA-30a, miRNA-24 and miRNA-21 are known to directly target Collagen I [137, 138], Snail [139] and the FAS ligand [140]. Accordingly, Let-7 and miR-30 family members, displaying renal regeneration properties [141, 142], were found enriched in MSC EVs. Some recent studies reported an increased level of LC3 II and Beclin 1 and a decreased level of p62 associated with the upregulation of miRNA-145 (miR-145) in human umbilical cord-MSCs co-cultured with renal epithelial cells (HK-2). Moreover, miR145 inhibit the phosphorylation of PI3K/AKT/mTOR, and to increase LC3B-positive staining as well as the autophagosome number [143]. miR29a, a well-known inhibitor of fibrosis, was shown to promote podocyte autophagy and to reduce apoptosis [144]. We observed that most of the MSC EV-miRNA targets are involved in autophagy as well as in pathways controlling this cascade, such as AMPK and mTOR [68]. Future experiments will be performed to elucidate the role of these miRNAs in the control of AMPK-ULK1 activation in tubular cells. Additionally, we noticed that MSC EVs deliver transcription factors such as CREBBP and PPARG, whose effectors are involved in pathways related to DN progression. The possibility that they can also contribute to the healing properties of MSC EVs will be further investigated.

Study limitations

DN is characterized by local inflammation that cause fibrosis and tissue remodelling [145]. This chronic inflammation is driven by different cell types of both the innate and adaptive systems. MSC-derived EV are known to exert also immunomodulatory effects on dendritic cells, T cells, B cells and macrophages [146] including the induction of T regulatory cells (Tregs). The investigation of the effect of MSC EVs in the modulation of the immune system is very intriguing and could provide evidence on new target that can be used in the clinical treatment. For example, the immunomodulatory effects of MSC-derived EV may influence leucocyte infiltration within the kidney, thus limiting renal function decline due to tissue inflammation. However, the use of immunocompromised mice did not allow the evaluation of this inflammatory component in the progression of DN. NSG strain infact is characterized by the lack mature T and B cells, and natural killer (NK) cells. NSG mice are also deficient in multiple cytokine signaling pathways, and they have many defects in innate immunity [147].

CONCLUSION

The results of the present study indicate that MSC EVs administered in a therapeutic-like schedule inhibit and revert the progression of functional and morphological renal dysfunction associated with diabetes. Molecular and bioinformatic analyses suggest that different mechanisms are involved in MSC EV treatment efficacy (anti-fibrotic and autophagy regulation). Validation of these mechanisms will be our future challenge.

Part of the data reported in this thesis are published in the paper: "Grange C, Tritta S, **Tapparo M**, et al. Stem cell-derived extracellular vesicles inhibit and revert fibrosis progression in a mouse model of diabetic nephropathy. *Sci Rep*. 2019;9(1):4468. Published 2019 Mar 14. doi:10.1038/s41598-019-41100-9"

REFERENCE

1. Tan SY, Mei Wong JL, Sim YJ, et al. Type 1 and 2 diabetes mellitus: A review on current treatment approach and gene therapy as potential intervention. Diabetes Metab Syndr. 2019 Jan-Feb;13(1):364-372. doi: 10.1016/j.dsx.2018.10.008.
2. Yu SM, Bonventre JV. Acute Kidney Injury and Progression of Diabetic Kidney Disease. *Adv Chronic Kidney Dis*. 2018;25(2):166-180. doi:10.1053/j.ackd.2017.12.005
3. Chen XM, Huang C, Pollock CA. Current opinion in the treatment of diabetic nephropathy. *Nephrol Open J*. 2015; 1(2): 20-24. doi: 10.17140/ NPOJ-1-104
4. Abecassis M, Bartlett ST, Collins AJ, et al. Kidney transplantation as primary therapy for end-stage renal disease: a National Kidney Foundation/Kidney Disease Outcomes Quality Initiative (NKF/KDOQITM) conference. *Clin J Am Soc Nephrol*. 2008;3(2):471-480. doi:10.2215/CJN.05021107
5. Gall MA, Hougaard P, Borch-Johnsen K, Parving HH. Risk factors for development of incipient and overt diabetic nephropathy in patients with non-insulin dependent diabetes mellitus: prospective, observational study. *BMJ*. 1997;314(7083):783-788. doi:10.1136/bmj.314.7083.783
6. Kidney Disease: Improving Global Outcomes (KDIGO) CKD WorkGroup. KDIGO 2012 clinical practice guideline for the evaluation and management of chronic kidney disease. Kidney Int Suppl. 2013;3: 1-150.
7. Edeling M, Ragi G, Huang S, Pavenstädt H, Susztak K. Developmental signalling pathways in renal fibrosis: the roles of Notch, Wnt and Hedgehog. *Nat Rev Nephrol*. 2016;12(7):426-439. doi:10.1038/nrneph.2016.54
8. Anil Kumar P, Welsh GI, Saleem MA, Menon RK. Molecular and cellular events mediating glomerular podocyte dysfunction and depletion in diabetes mellitus. *Front Endocrinol (Lausanne)*. 2014;5:151. Published 2014 Sep 25. doi:10.3389/fendo.2014.00151
9. Anders HJ. Immune system modulation of kidney regeneration--mechanisms and implications. *Nat Rev Nephrol*. 2014;10(6):347-358. doi:10.1038/nrneph.2014.68
10. Doublier S, Salvidio G, Lupia E, et al. Nephrin expression is reduced in human diabetic nephropathy: evidence for a distinct role for glycated albumin and angiotensin II. *Diabetes*. 2003;52(4):1023-1030. doi:10.2337/diabetes.52.4.1023
11. Wolf G, Ziyadeh F, N: Cellular and Molecular Mechanisms of Proteinuria in Diabetic Nephropathy. Nephron Physiol 2007;106:p26-p31. Doi: 10.1159/000101797

12. Lin CL, Lee PH, Hsu YC et al. MicroRNA-29a promotion of nephrin acetylation ameliorates hyperglycemia-induced podocyte dysfunction. J. Am. Soc. Nephrol. 2014; 25: 1698–709.
13. Bonventre JV. Can we target tubular damage to prevent renal function decline in diabetes?. *Semin Nephrol*. 2012;32(5):452-462. doi:10.1016/j.semnephrol.2012.07.008
14. Vaidya VS, Niewczas MA, Ficociello LH, et al. Regression of microalbuminuria in type 1 diabetes is associated with lower levels of urinary tubular injury biomarkers, kidney injury molecule-1, and N-acetyl-β-D-glucosaminidase. *Kidney Int*. 2011;79(4):464-470. doi:10.1038/ki.2010.404
15. Waikar SS, Sabbisetti V, Ärnlöv J, et al. Relationship of proximal tubular injury to chronic kidney disease as assessed by urinary kidney injury molecule-1 in five cohort studies. *Nephrol Dial Transplant*. 2016;31(9):1460-1470. doi:10.1093/ndt/gfw203
16. Mora-Fernández C, Domínguez-Pimentel V, de Fuentes MM, Górriz JL, Martínez-Castelao A, Navarro-González JF. Diabetic kidney disease: from physiology to therapeutics. *J Physiol*. 2014;592(18):3997-4012. doi:10.1113/jphysiol.2014.272328
17. Badal SS, Danesh FR. New insights into molecular mechanisms of diabetic kidney disease. *Am J Kidney Dis*. 2014; 63: S63-S83. doi: 10.1053/j.ajkd.2013.10.047
18. Forbes JM, Coughlan MT, Cooper ME. Oxidative stress as a major culprit in kidney disease in diabetes. *Diabetes*. 2008;57(6):1446-1454. doi:10.2337/db08-0057
19. Advani A, Gilbert RE. The endothelium in diabetic nephropathy. *Semin Nephrol*. 2012;32(2):199-207. doi:10.1016/j.semnephrol.2012.02.006
20. Tessari P. Nitric oxide in the normal kidney and in patients with diabetic nephropathy. *J Nephrol*. 2015;28(3):257-268. doi:10.1007/s40620-014-0136-2
21. Artunc F, Schleicher E, Weigert C, Fritsche A, Stefan N, Haring HU. The impact of insulin resistance on the kidney and vasculature. Nat Rev Nephrol. 2016; 12(12):721–737.
22. Zanchi A, Moczulski DK, Hanna LS, Wantman M, Warram JH, Krolewski AS. Risk of advanced diabetic nephropathy in type 1 diabetes is associated with endothelial nitric oxide synthase gene polymorphism. Kidney Int. 2000; 57(2):405–413.
23. Lim AKh. Diabetic nephropathy - complications and treatment. *Int J Nephrol Renovasc Dis*. 2014;7:361-381. Published 2014 Oct 15. doi:10.2147/IJNRD.S40172
24. Zhang YY, Yu Y, Yu C. Antifibrotic Roles of RAAS Blockers: Update. *Adv Exp Med Biol*. 2019;1165:671-691. doi:10.1007/978-981-13-8871-2_33
25. Perkins BA, Ficociello LH, Roshan B, Warram JH, Krolewski AS. In patients with type 1 diabetes and new-onset microalbuminuria the development of advanced chronic kidney

disease may not require progression to proteinuria. *Kidney Int*. 2010;77(1):57-64. doi:10.1038/ki.2009.399

26. Hargrove GM, Dufresne J, Whiteside C, Muruve DA, Wong NC. Diabetes mellitus increases endothelin-1 gene transcription in rat kidney. *Kidney Int*. 2000;58(4):1534-1545. doi:10.1046/j.1523-1755.2000.00315.x
27. Lee SY, Kim SI, Choi ME. Therapeutic targets for treating fibrotic kidney diseases. Transl Res. 2015 Apr;165(4):512-30. doi: 10.1016/j.trsl.2014.07.010.
28. Ho FM, Liu SH, Liau CS, Huang PJ, Lin-Shiau SY. High glucose-induced apoptosis in human endothelial cells is mediated by sequential activations of c-Jun NH(2)-terminal kinase and caspase-3. *Circulation*. 2000;101(22):2618-2624. doi:10.1161/01.cir.101.22.2618
29. Kramann R, Wongboonsin J, Chang-Panesso M, Machado FG, Humphreys BD. Gli1^{+} Pericyte Loss Induces Capillary Rarefaction and Proximal Tubular Injury. *J Am Soc Nephrol*. 2017;28(3):776-784. doi:10.1681/ASN.2016030297
30. Gnudi L, Benedetti S, Woolf AS, Long DA. Vascular growth factors play critical roles in kidney glomeruli. *Clin Sci (Lond)*. 2015;129(12):1225-1236. doi:10.1042/CS20150403
31. Veron D, Reidy KJ, Bertuccio C, et al. Overexpression of VEGF-A in podocytes of adult mice causes glomerular disease. *Kidney Int*. 2010;77(11):989-999. doi:10.1038/ki.2010.64
32. Singh DK, Winocour P, Farrington K. Mechanisms of disease: the hypoxic tubular hypothesis of diabetic nephropathy. *Nat Clin Pract Nephrol*. 2008;4(4):216-226. doi:10.1038/ncpneph0757
33. Higgins DF, Kimura K, Bernhardt WM, et al. Hypoxia promotes fibrogenesis in vivo via HIF-1 stimulation of epithelial-to-mesenchymal transition. *J Clin Invest*. 2007;117(12):3810-3820. doi:10.1172/JCI30487
34. Sharma K. Mitochondrial hormesis and diabetic complications. *Diabetes*. 2015;64(3):663-672. doi:10.2337/db14-0874
35. Sheetz MJ, King GL. Molecular understanding of hyperglycemia's adverse effects for diabetic complications. *JAMA*. 2002;288(20):2579-2588. doi:10.1001/jama.288.20.2579
36. Ha H, Lee HB. Reactive oxygen species as glucose signaling molecules in mesangial cells cultured under high glucose. *Kidney Int Suppl*. 2000;77:S19-S25. doi:10.1046/j.1523-1755.2000.07704.x
37. Srivastava SK, Ramana KV, Bhatnagar A. Role of aldose reductase and oxidative damage in diabetes and the consequent potential for therapeutic options. *Endocr Rev*. 2005;26(3):380-392. doi:10.1210/er.2004-0028

38. Tang SC, Leung JC, Chan LY, Tsang AW, Lai KN. Activation of tubular epithelial cells in diabetic nephropathy and the role of the peroxisome proliferator-activated receptor-gamma agonist. *J Am Soc Nephrol*. 2006;17(6):1633-1643. doi:10.1681/ASN.2005101113
39. Tang SC, Chan LY, Leung JC, et al. Differential effects of advanced glycation end-products on renal tubular cell inflammation. *Nephrology (Carlton)*. 2011;16(4):417-425. doi:10.1111/j.1440-1797.2010.01437.x
40. Navarro-González JF, Mora-Fernández C, Muros de Fuentes M, García-Pérez J. Inflammatory molecules and pathways in the pathogenesis of diabetic nephropathy. *Nat Rev Nephrol*. 2011;7(6):327-340. doi:10.1038/nrneph.2011.51
41. Wu CC, Sytwu HK, Lu KC, Lin YF. Role of T cells in type 2 diabetic nephropathy. *Exp Diabetes Res*. 2011;2011:514738. doi:10.1155/2011/514738
42. Tang S, Leung JC, Abe K, et al. Albumin stimulates interleukin-8 expression in proximal tubular epithelial cells in vitro and in vivo. *J Clin Invest*. 2003;111(4):515-527. doi:10.1172/JCI16079
43. Noh H, King GL. The role of protein kinase C activation in diabetic nephropathy. *Kidney Int Suppl*. 2007;(106):S49-S53. doi:10.1038/sj.ki.5002386
44. Sakai N, Wada T, Furuichi K, et al. Involvement of extracellular signal-regulated kinase and p38 in human diabetic nephropathy. *Am J Kidney Dis*. 2005;45(1):54-65. doi:10.1053/j.ajkd.2004.08.039
45. Schmid H, Boucherot A, Yasuda Y, et al. Modular activation of nuclear factor-kappaB transcriptional programs in human diabetic nephropathy. *Diabetes*. 2006;55(11):2993-3003. doi:10.2337/db06-0477
46. Lim AKh. Diabetic nephropathy - complications and treatment. *Int J Nephrol Renovasc Dis*. 2014;7:361-381. Published 2014 Oct 15. doi:10.2147/IJNRD.S40172
47. Nath KA. Tubulointerstitial changes as a major determinant in the progression of renal damage. *Am J Kidney Dis*. 1992;20(1):1-17. doi:10.1016/s0272-6386(12)80312-x
48. Simonson MS. Phenotypic transitions and fibrosis in diabetic nephropathy. *Kidney Int*. 2007;71(9):846-854. doi:10.1038/sj.ki.5002180
49. Liu Y. Cellular and molecular mechanisms of renal fibrosis. *Nat Rev Nephrol*. 2011;7(12):684-696. Published 2011 Oct 18. doi:10.1038/nrneph.2011.149
50. Zhang L, Pang S, Deng B, Qian L, Chen J, Zou J et al (2012) High glucose induces renal mesangial cell proliferation and fibronectin expression through JNK/NF-κB/NADPHoxidase/ROSpathway, which is inhibited by resveratrol. Int J Biochem Cell Biol 44:629–638

51. Ovadya Y, Krizhanovsky V. A new Twist in kidney fibrosis. *Nat Med*. 2015;21(9):975-977. doi:10.1038/nm.3938
52. Yuan Q, Tan RJ, Liu Y. Myofibroblast in Kidney Fibrosis: Origin, Activation, and Regulation. *Adv Exp Med Biol*. 2019;1165:253-283. doi:10.1007/978-981-13-8871-2_12
53. Ziyadeh FN, Snipes ER, Watanabe M, Alvarez RJ, Goldfarb S, Haverty TP. High glucose induces cell hypertrophy and stimulates collagen gene transcription in proximal tubule. *Am J Physiol*. 1990;259(4 Pt 2):F704-F714. doi:10.1152/ajprenal.1990.259.4.F704
54. Rocco MV, Chen Y, Goldfarb S, Ziyadeh FN. Elevated glucose stimulates TGF-beta gene expression and bioactivity in proximal tubule. *Kidney Int*. 1992;41(1):107-114. doi:10.1038/ki.1992.14
55. Liu Q, Xing L, Wang L, et al. Therapeutic effects of suppressors of cytokine signaling in diabetic nephropathy. *J Histochem Cytochem*. 2014;62(2):119-128. doi:10.1369/0022155413512493
56. Hills CE, Siamantouras E, Smith SW, Cockwell P, Liu KK, Squires PE. TGFβ modulates cell-to-cell communication in early epithelial-to-mesenchymal transition. *Diabetologia*. 2012;55(3):812-824. doi:10.1007/s00125-011-2409-9
57. Meng XM, Chung AC, Lan HY. Role of the TGF-β/BMP-7/Smad pathways in renal diseases. *Clin Sci (Lond)*. 2013;124(4):243-254. doi:10.1042/CS20120252
58. Wu CF, Chiang WC, Lai CF, et al. Transforming growth factor β-1 stimulates profibrotic epithelial signaling to activate pericyte-myofibroblast transition in obstructive kidney fibrosis. *Am J Pathol*. 2013;182(1):118-131. doi:10.1016/j.ajpath.2012.09.009
59. Böttinger EP, Bitzer M. TGF-beta signaling in renal disease. *J Am Soc Nephrol*. 2002;13(10):2600-2610. doi:10.1097/01.asn.0000033611.79556.ae
60. López-Hernández FJ, López-Novoa JM. Role of TGF-β in chronic kidney disease: an integration of tubular, glomerular and vascular effects. *Cell Tissue Res*. 2012;347(1):141-154. doi:10.1007/s00441-011-1275-6
61. Xu W, Yang Z, Lu N. A new role for the PI3K/Akt signaling pathway in the epithelial-mesenchymal transition. *Cell Adh Migr*. 2015;9(4):317-324. doi:10.1080/19336918.2015.1016686
62. Xie X, Xia W, Fei X, et al. Relaxin Inhibits High Glucose-Induced Matrix Accumulation in Human Mesangial Cells by Interfering with TGF-β1 Production and Mesangial Cells Phenotypic Transition. *Biol Pharm Bull*. 2015;38(10):1464-1469. doi:10.1248/bpb.b15-00127

63. Zhu L, Zhao S, Liu S, Liu Q, Li F, Hao J. PTEN Regulates Renal Extracellular Matrix Deposit via Increased CTGF in Diabetes Mellitus. *J Cell Biochem*. 2016;117(5):1187-1198. doi:10.1002/jcb.25402
64. Brosius FC, Tuttle KR, Kretzler M. JAK inhibition in the treatment of diabetic kidney disease. *Diabetologia*. 2016;59(8):1624-1627. doi:10.1007/s00125-016-4021-5
65. Hwang I, Seo EY, Ha H. Wnt/beta-catenin signaling: a novel target for therapeutic intervention of fibrotic kidney disease. *Arch Pharm Res*. 2009;32(12):1653-1662. doi:10.1007/s12272-009-2200-3
66. Zhou T, He X, Cheng R, et al. Implication of dysregulation of the canonical wingless-type MMTV integration site (WNT) pathway in diabetic nephropathy. *Diabetologia*. 2012;55(1):255-266. doi:10.1007/s00125-011-2314-2
67. Liu Y. New insights into epithelial-mesenchymal transition in kidney fibrosis. *J Am Soc Nephrol*. 2010;21(2):212-222. doi:10.1681/ASN.2008121226
68. Zhao XC, Livingston MJ, Liang XL, Dong Z. Cell Apoptosis and Autophagy in Renal Fibrosis. *Adv Exp Med Biol*. 2019;1165:557-584. doi:10.1007/978-981-13-8871-2_28
69. Klionsky DJ, Baehrecke EH, Brumell JH, et al. A comprehensive glossary of autophagy-related molecules and processes (2nd edition). *Autophagy*. 2011;7(11):1273-1294. doi:10.4161/auto.7.11.17661
70. Hansen M, Rubinsztein DC, Walker DW. Autophagy as a promoter of longevity: insights from model organisms [published correction appears in Nat Rev Mol Cell Biol. 2018 Jul 25;:]. *Nat Rev Mol Cell Biol*. 2018;19(9):579-593. doi:10.1038/s41580-018-0033-y
71. Livingston MJ, Ding HF, Huang S, Hill JA, Yin XM, Dong Z. Persistent activation of autophagy in kidney tubular cells promotes renal interstitial fibrosis during unilateral ureteral obstruction. *Autophagy*. 2016;12(6):976-998. doi:10.1080/15548627.2016.1166317
72. Huber TB, Edelstein CL, Hartleben B, et al. Emerging role of autophagy in kidney function, diseases and aging. *Autophagy*. 2012;8(7):1009-1031. doi:10.4161/auto.19821
73. Mallat A, Lodder J, Teixeira-Clerc F, Moreau R, Codogno P, Lotersztajn S. Autophagy: a multifaceted partner in liver fibrosis. *Biomed Res Int*. 2014;2014:869390. doi:10.1155/2014/869390
74. Araya J, Kojima J, Takasaka N, et al. Insufficient autophagy in idiopathic pulmonary fibrosis. *Am J Physiol Lung Cell Mol Physiol*. 2013;304(1):L56-L69. doi:10.1152/ajplung.00213.2012
75. Forbes MS, Thornhill BA, Chevalier RL. Proximal tubular injury and rapid formation of atubular glomeruli in mice with unilateral ureteral obstruction: a new look at an old

model. *Am J Physiol Renal Physiol*. 2011;301(1):F110-F117. doi:10.1152/ajprenal.00022.2011

76. Koesters R, Kaissling B, Lehir M, et al. Tubular overexpression of transforming growth factor-beta1 induces autophagy and fibrosis but not mesenchymal transition of renal epithelial cells. *Am J Pathol*. 2010;177(2):632-643. doi:10.2353/ajpath.2010.091012
77. Ding Y, Kim Sl, Lee SY, Koo JK, Wang Z, Choi ME. Autophagy regulates TGF-β expression and suppresses kidney fibrosis induced by unilateral ureteral obstruction. *J Am Soc Nephrol*. 2014;25(12):2835-2846. doi:10.1681/ASN.2013101068
78. Ding Y, Kim JK, Kim SI, et al. TGF-beta1 protects against mesangial cell apoptosis via induction of autophagy. *J Biol Chem*. 2010;285(48):37909-37919. doi:10.1074/jbc.M109.093724
79. Sakaguchi M, Isono M, Isshiki K, Sugimoto T, Koya D, Kashiwagi A. Inhibition of mTOR signaling with rapamycin attenuates renal hypertrophy in the early diabetic mice. *Biochem Biophys Res Commun*. 2006;340(1):296-301. doi:10.1016/j.bbrc.2005.12.012
80. Jin Y, Liu S, Ma Q, Xiao D, Chen L. Berberine enhances the AMPK activation and autophagy and mitigates high glucose-induced apoptosis of mouse podocytes. *Eur J Pharmacol*. 2017;794:106-114. doi:10.1016/j.ejphar.2016.11.037
81. Hasegawa K, Wakino S, Simic P, et al. Renal tubular Sirt1 attenuates diabetic albuminuria by epigenetically suppressing Claudin-1 overexpression in podocytes. *Nat Med*. 2013;19(11):1496-1504. doi:10.1038/nm.3363
82. Levine B, Kroemer G. Autophagy in the pathogenesis of disease. *Cell*. 2008;132(1):27-42. doi:10.1016/j.cell.2007.12.018
83. Lenoir O, Jasiek M, Hénique C, et al. Endothelial cell and podocyte autophagy synergistically protect from diabetes-induced glomerulosclerosis. *Autophagy*. 2015;11(7):1130-1145. doi:10.1080/15548627.2015.1049799
84. Camussi G, Deregibus MC, Bruno S, Cantaluppi V, Biancone L. Exosomes/microvesicles as a mechanism of cell-to-cell communication. *Kidney Int*. 2010;78(9):838-848. doi:10.1038/ki.2010.278
85. Derkus B, Emregul KC, Emregul E. A new approach in stem cell research-Exosomes: Their mechanism of action via cellular pathways. *Cell Biol Int*. 2017;41(5):466-475. doi:10.1002/cbin.10742
86. Eirin A, Zhu XY, Puranik AS, et al. Mesenchymal stem cell-derived extracellular vesicles attenuate kidney inflammation. *Kidney Int*. 2017;92(1):114-124. doi:10.1016/j.kint.2016.12.023

87. Giebel B, Kordelas L, Börger V. Clinical potential of mesenchymal stem/stromal cell-derived extracellular vesicles. *Stem Cell Investig*. 2017;4:84. Published 2017 Oct 24. doi:10.21037/sci.2017.09.06
88. Bruno S, Grange C, Deregibus MC, et al. Mesenchymal stem cell-derived microvesicles protect against acute tubular injury. *J Am Soc Nephrol*. 2009;20(5):1053-1067. doi:10.1681/ASN.2008070798
89. Herrera Sanchez MB, Bruno S, Grange C, et al. Human liver stem cells and derived extracellular vesicles improve recovery in a murine model of acute kidney injury. *Stem Cell Res Ther*. 2014;5(6):124. Published 2014 Nov 10. doi:10.1186/scrt514
90. Grange C, Iampietro C, Bussolati B. Stem cell extracellular vesicles and kidney injury. *Stem Cell Investig*. 2017;4:90. Published 2017 Nov 16. doi:10.21037/sci.2017.11.02
91. He J, Wang Y, Lu X, et al. Micro-vesicles derived from bone marrow stem cells protect the kidney both in vivo and in vitro by microRNA-dependent repairing [published correction appears in Nephrology (Carlton). 2016 Apr;21(4):347]. *Nephrology (Carlton)*. 2015;20(9):591-600. doi:10.1111/nep.12490
92. He J, Wang Y, Sun S, et al. Bone marrow stem cells-derived microvesicles protect against renal injury in the mouse remnant kidney model. *Nephrology (Carlton)*. 2012;17(5):493-500. doi:10.1111/j.1440-1797.2012.01589.x
93. Kholia S, Herrera Sanchez MB, Cedrino M, et al. Human Liver Stem Cell-Derived Extracellular Vesicles Prevent Aristolochic Acid-Induced Kidney Fibrosis. *Front Immunol*. 2018;9:1639. Published 2018 Jul 19. doi:10.3389/fimmu.2018.01639
94. Kholia S, Herrera Sanchez MB, Cedrino M, et al. Mesenchymal Stem Cell Derived Extracellular Vesicles Ameliorate Kidney Injury in Aristolochic Acid Nephropathy. *Front Cell Dev Biol*. 2020;8:188. Published 2020 Mar 24. doi:10.3389/fcell.2020.00188
95. Jiang ZZ, Liu YM, Niu X, et al. Exosomes secreted by human urine-derived stem cells could prevent kidney complications from type I diabetes in rats. *Stem Cell Res Ther*. 2016;7:24. Published 2016 Feb 6. doi:10.1186/s13287-016-0287-2
96. Nagaishi K, Mizue Y, Chikenji T, et al. Mesenchymal stem cell therapy ameliorates diabetic nephropathy via the paracrine effect of renal trophic factors including exosomes. *Sci Rep*. 2016;6:34842. Published 2016 Oct 10. doi:10.1038/srep34842
97. Viñas JL, Burger D, Zimpelmann J, Haneef R, Knoll W, Campbell P et al (2016) Transfer of microRNA-486-5p from human endothelial colony forming cell-derived exosomes reduces ischemic kidney injury. Kidney Int 90:1238–1250
98. Cantaluppi V, Gatti S, Medica D, Figliolini F, Bruno S, Deregibus MC et al (2012) Microvesicles derived from endothelial progenitor cells protect the kidney from

ischemia-reperfusion injury by microRNA-dependent reprogramming of resident renal cells. Kidney Int 82:412–427

99. Cantaluppi V, Medica D, Mannari C, Stiaccini G, Figliolini F, Dellepiane S et al (2014) Endothelial progenitor cell-derived extracellular vesicles protect from complement-mediated mesangial injury in experimental anti-Thy1.1 glomerulonephritis. Nephrol Dial Transplant 30:410–422

100. Dominguez JH, Liu Y, Gao H, Dominguez JM 2nd, Xie D, Kelly KJ (2017) Renal tubular cellderived extracellular vesicles accelerate the recovery of established renal ischemia reperfusioninjury. J Am Soc Nephrol 28:3533–3544

101. Ebrahim N, Ahmed IA, Hussien NI, et al. Mesenchymal Stem Cell-Derived Exosomes Ameliorated Diabetic Nephropathy by Autophagy Induction through the mTOR Signaling Pathway. *Cells*. 2018;7(12):226. Published 2018 Nov 22. doi:10.3390/cells7120226

102. Jin J, Shi Y, Gong J, et al. Exosome secreted from adipose-derived stem cells attenuates diabetic nephropathy by promoting autophagy flux and inhibiting apoptosis in podocyte. *Stem Cell Res Ther*. 2019;10(1):95. Published 2019 Mar 15. doi:10.1186/s13287-019-1177-1

103. Collino F, Bruno S, Incarnato D, Dettori D, Neri F, Provero P, Pomatto M, Oliviero S, Tetta C, Quesenberry PJ, Camussi G. AKI Recovery Induced by Mesenchymal Stromal Cell-Derived Extracellular Vesicles Carrying MicroRNAs. J Am Soc Nephrol. 2015 Oct;26(10):2349-60. doi: 10.1681/ASN.2014070710.

104. Sticht C, De La Torre C, Parveen A, Gretz N. miRWalk: An online resource for prediction of microRNA binding sites. *PLoS One*. 2018;13(10):e0206239. Published 2018 Oct 18. doi:10.1371/journal.pone.0206239

105. Pathan M, Keerthikumar S, Chisanga D, et al. A novel community driven software for functional enrichment analysis of extracellular vesicles data. *J Extracell Vesicles*. 2017;6(1):1321455. Published 2017 May 26. doi:10.1080/20013078.2017.1321455

106. Han H, Cho JW, Lee S, et al. TRRUST v2: an expanded reference database of human and mouse transcriptional regulatory interactions. *Nucleic Acids Res*. 2018;46(D1):D380-D386. doi:10.1093/nar/gkx1013

107. Pearson T, Shultz LD, Lief J, et al. A new immunodeficient hyperglycaemic mouse model based on the Ins2Akita mutation for analyses of human islet and beta stem and progenitor cell function. *Diabetologia*. 2008;51(8):1449-1456. doi:10.1007/s00125-008-1057-1

108. Morishita Y, Imai T, Yoshizawa H, et al. Delivery of microRNA-146a with polyethylenimine nanoparticles inhibits renal fibrosis in vivo. *Int J Nanomedicine*. 2015;10:3475-3488. Published 2015 May 11. doi:10.2147/IJN.S82587

109. Bhatt K, Lanting LL, Jia Y, et al. Anti-Inflammatory Role of MicroRNA-146a in the Pathogenesis of Diabetic Nephropathy. *J Am Soc Nephrol*. 2016;27(8):2277-2288. doi:10.1681/ASN.2015010111

110. Park JH, Hwang I, Hwang SH, Han H, Ha H. Human umbilical cord blood-derived mesenchymal stem cells prevent diabetic renal injury through paracrine action. *Diabetes Res Clin Pract*. 2012;98(3):465-473. doi:10.1016/j.diabres.2012.09.034

111. Ni W, Fang Y, Xie L, et al. Adipose-Derived Mesenchymal Stem Cells Transplantation Alleviates Renal Injury in Streptozotocin-Induced Diabetic Nephropathy. *J Histochem Cytochem*. 2015;63(11):842-853. doi:10.1369/0022155415599039

112. Lv SS, Liu G, Wang JP, et al. Mesenchymal stem cells transplantation ameliorates glomerular injury in streptozotocin-induced diabetic nephropathy in rats via inhibiting macrophage infiltration. *Int Immunopharmacol*. 2013;17(2):275-282. doi:10.1016/j.intimp.2013.05.031

113. Sedrakyan S, Da Sacco S, Milanesi A, et al. Injection of amniotic fluid stem cells delays progression of renal fibrosis. *J Am Soc Nephrol*. 2012;23(4):661-673. doi:10.1681/ASN.2011030243

114. Vader P, Mol EA, Pasterkamp G, Schiffelers RM. Extracellular vesicles for drug delivery. *Adv Drug Deliv Rev*. 2016;106(Pt A):148-156. doi:10.1016/j.addr.2016.02.006

115. Ortiz LA, Gambelli F, McBride C, et al. Mesenchymal stem cell engraftment in lung is enhanced in response to bleomycin exposure and ameliorates its fibrotic effects. *Proc Natl Acad Sci U S A*. 2003;100(14):8407-8411. doi:10.1073/pnas.1432929100

116. Kidd S, Spaeth E, Dembinski JL, et al. Direct evidence of mesenchymal stem cell tropism for tumor and wounding microenvironments using in vivo bioluminescent imaging. *Stem Cells*. 2009;27(10):2614-2623. doi:10.1002/stem.187

117. Grange C, Tapparo M, Bruno S, et al. Biodistribution of mesenchymal stem cell-derived extracellular vesicles in a model of acute kidney injury monitored by optical imaging. *Int J Mol Med*. 2014;33(5):1055-1063. doi:10.3892/ijmm.2014.1663

118. Keshtkar S, Azarpira N, Ghahremani MH. Mesenchymal stem cell-derived extracellular vesicles: novel frontiers in regenerative medicine. *Stem Cell Res Ther*. 2018;9(1):63. Published 2018 Mar 9. doi:10.1186/s13287-018-0791-7

119. Bruno S, Camussi G. Exploring mesenchymal stem cell-derived extracellular vesicles in acute kidney injury. *Methods Mol Biol*. 2014;1213:139-145. doi:10.1007/978-1-4939-1453-1_12

120. Bruno S, Grange C, Collino F, et al. Microvesicles derived from mesenchymal stem cells enhance survival in a lethal model of acute kidney injury. *PLoS One*. 2012;7(3):e33115. doi:10.1371/journal.pone.0033115

121. Zhou Y, Xu H, Xu W, et al. Exosomes released by human umbilical cord mesenchymal stem cells protect against cisplatin-induced renal oxidative stress and apoptosis in vivo and in vitro. *Stem Cell Res Ther*. 2013;4(2):34. Published 2013 Apr 25. doi:10.1186/scrt194

122. Bai X, Geng J, Zhou Z, Tian J, Li X. MicroRNA-130b improves renal tubulointerstitial fibrosis via repression of Snail-induced epithelial-mesenchymal transition in diabetic nephropathy. *Sci Rep*. 2016;6:20475. Published 2016 Feb 3. doi:10.1038/srep20475

123. Ohnuki K, Umezono T, Abe M, et al. Expression of transcription factor Snai1 and tubulointerstitial fibrosis in progressive nephropathy. *J Nephrol*. 2012;25(2):233-239. doi:10.5301/JN.2011.8449

124. Xu X, Xiao L, Xiao P, et al. A glimpse of matrix metalloproteinases in diabetic nephropathy. *Curr Med Chem*. 2014;21(28):3244-3260. doi:10.2174/09298673216661407160920 52

125. Mason RM, Wahab NA. Extracellular matrix metabolism in diabetic nephropathy. *J Am Soc Nephrol*. 2003;14(5):1358-1373. doi:10.1097/01.asn.0000065640.77499.d7

126. McLennan SV, Kelly DJ, Cox AJ, et al. Decreased matrix degradation in diabetic nephropathy: effects of ACE inhibition on the expression and activities of matrix metalloproteinases. *Diabetologia*. 2002;45(2):268-275. doi:10.1007/s00125-001-0730-4

127. Jin J, Ku YH, Kim Y, et al. Differential proteome profiling using iTRAQ in microalbuminuric and normoalbuminuric type 2 diabetic patients. *Exp Diabetes Res*. 2012;2012:168602. doi:10.1155/2012/168602

128. Conserva F, Gesualdo L, Papale M. A Systems Biology Overview on Human Diabetic Nephropathy: From Genetic Susceptibility to Post-Transcriptional and Post-Translational Modifications. *J Diabetes Res*. 2016;2016:7934504. doi:10.1155/2016/7934504

129. Ortiz A, Lorz C, González-Cuadrado S, Garcia del Moral R, O'Valle F, Egido J. Cytokines and Fas regulate apoptosis in murine renal interstitial fibroblasts. *J Am Soc Nephrol*. 1997;8(12):1845-1854.

130. Yang CW, Faulkner GR, Wahba IM, et al. Expression of apoptosis-related genes in chronic cyclosporine nephrotoxicity in mice. *Am J Transplant*. 2002;2(5):391-399. doi:10.1034/j.1600-6143.2002.20501.x
131. Chung AC, Lan HY. Chemokines in renal injury. *J Am Soc Nephrol*. 2011;22(5):802-809. doi:10.1681/ASN.2010050510
132. Hernández-Gea V, Ghiassi-Nejad Z, Rozenfeld R, et al. Autophagy releases lipid that promotes fibrogenesis by activated hepatic stellate cells in mice and in human tissues. *Gastroenterology*. 2012;142(4):938-946. doi:10.1053/j.gastro.2011.12.044
133. Patel AS, Lin L, Geyer A, et al. Autophagy in idiopathic pulmonary fibrosis. *PLoS One*. 2012;7(7):e41394. doi:10.1371/journal.pone.0041394
134. Kim WY, Nam SA, Song HC, et al. The role of autophagy in unilateral ureteral obstruction rat model. *Nephrology (Carlton)*. 2012;17(2):148-159. doi:10.1111/j.1440-1797.2011.01541.x
135. Bruno S, Tapparo M, Collino F, et al. Renal Regenerative Potential of Different Extracellular Vesicle Populations Derived from Bone Marrow Mesenchymal Stromal Cells. *Tissue Eng Part A*. 2017;23(21-22):1262-1273. doi:10.1089/ten.TEA.2017.0069
136. Collino F, Pomatto M, Bruno S, et al. Exosome and Microvesicle-Enriched Fractions Isolated from Mesenchymal Stem Cells by Gradient Separation Showed Different Molecular Signatures and Functions on Renal Tubular Epithelial Cells. *Stem Cell Rev Rep*. 2017;13(2):226-243. doi:10.1007/s12015-016-9713-1
137. Schug J, McKenna LB, Walton G, et al. Dynamic recruitment of microRNAs to their mRNA targets in the regenerating liver. *BMC Genomics*. 2013;14:264. Published 2013 Apr 18. doi:10.1186/1471-2164-14-264
138. Balakrishnan I, Yang X, Brown J, et al. Genome-wide analysis of miRNA-mRNA interactions in marrow stromal cells. *Stem Cells*. 2014;32(3):662-673. doi:10.1002/stem.1531
139. Zhang J, Zhang H, Liu J, et al. miR-30 inhibits TGF-β1-induced epithelial-to-mesenchymal transition in hepatocyte by targeting Snail1. *Biochem Biophys Res Commun*. 2012;417(3):1100-1105. doi:10.1016/j.bbrc.2011.12.121
140. Sayed D, He M, Hong C, et al. MicroRNA-21 is a downstream effector of AKT that mediates its antiapoptotic effects via suppression of Fas ligand. *J Biol Chem*. 2010;285(26):20281-20290. doi:10.1074/jbc.M110.109207
141. Park JT, Kato M, Lanting L, et al. Repression of let-7 by transforming growth factor-β1-induced Lin28 upregulates collagen expression in glomerular mesangial cells under

diabetic conditions. *Am J Physiol Renal Physiol*. 2014;307(12):F1390-F1403. doi:10.1152/ajprenal.00458.2014

142. Gu D, Zou X, Ju G, Zhang G, Bao E, Zhu Y. Mesenchymal Stromal Cells Derived Extracellular Vesicles Ameliorate Acute Renal Ischemia Reperfusion Injury by Inhibition of Mitochondrial Fission through miR-30. *Stem Cells Int*. 2016;2016:2093940. doi:10.1155/2016/2093940
143. Xiang J, Jiang T, Zhang W, Xie W, Tang X, Zhang J. Human umbilical cord-derived mesenchymal stem cells enhanced HK-2 cell autophagy through MicroRNA-145 by inhibiting the PI3K/AKT/mTOR signaling pathway. *Exp Cell Res*. 2019;378(2):198-205. doi:10.1016/j.yexcr.2019.03.019
144. Fan WX, Wen XL, Xiao H, Yang QP, Liang Z. MicroRNA-29a enhances autophagy in podocytes as a protective mechanism against high glucose-induced apoptosis by targeting heme oxygenase-1. *Eur Rev Med Pharmacol Sci*. 2018;22(24):8909-8917. doi:10.26355/eurrev_201812_16660
145. Zheng Z, Zheng F. Immune Cells and Inflammation in Diabetic Nephropathy. J Diabetes Res. 2016;2016:1841690. doi: 10.1155/2016/1841690. Epub 2015 Dec 28. PMID: 26824038; PMCID: PMC4707326.
146. Uccelli A, Moretta L, Pistoia V. Mesenchymal stem cells in health and disease. Nat Rev Immunol. 2008 Sep; 8(9):726-36
147. Breyer MD, Böttinger E, Brosius FC 3rd, Coffman TM, Harris RC, Heilig CW, Sharma K; AMDCC. Mouse models of diabetic nephropathy. J Am Soc Nephrol. 2005 Jan;16(1):27-45. doi: 10.1681/ASN.2004080648. Epub 2004 Nov 24. PMID: 15563560.